REVIEW

National Science Review
1: 119–143, 2014
doi: 10.1093/nsr/nwt028
Advance access publication 31 December 2013

GEOSCIENCES

Long-term cycles in the carbon reservoir of the Quaternary ocean: a perspective from the South China Sea

PinXian Wang*, QianYu Li, Jun Tian, ZhiMin Jian, ChuanLian Liu, Li Li and WenTao Ma

ABSTRACT

In recent years, long-term, high-resolution records from the deep sea and ice-cores have offered new research opportunities for Quaternary science. Paleoclimate studies are no longer restricted to individual glacial cycles, but extend to long-term ($\geq 10^5$ yr) processes across those cycles. Ocean Drilling Program Leg 184 of the South China Sea in 1999 uncovered well-preserved sediment sections, in which three long-term cycles in Pleistocene carbon isotope ($\delta^{13}C$) sequence have been found and demonstrated to be common in the global ocean. Subsequent discoveries confirm the existence of long-term processes of 10^5 yr in both the hydrologic (ice-sheet changes) and carbon (biogeochemical changes) cycles, posing the question whether the two processes are related. The present review shows that the long-eccentricity cycles prevail throughout the $\delta^{13}C$ and other biogeochemical records in geologic history, and 400-kyr cycles in the oceanic $\delta^{13}C$ sequence before the Quaternary can be hypothetically explained by changes in ratio between particulate and dissolved organic carbon (POC/DOC) in the ocean, depending on the monsoon-controlled nutrient supply. This is a 'DOC hypothesis'. However, ocean restructuring at 1.6 Ma marked by the isolation of a sluggish abyss under the Southern Ocean has obscured the long-eccentricity 400-kyr signal in oceanic $\delta^{13}C$. The last million-year period has experienced two major changes in the climate regime, namely the mid-Pleistocene transition (MPT) centered at 0.9 Ma and the mid-Brunhes event (MBE) around 0.4 Ma. The MPT and MBE were preluded by $\delta^{13}C$ maxima-III ($\delta^{13}C_{max\text{-}III}$) $\sim$ 1.0 Ma and $\delta^{13}C_{max\text{-}II}$ $\sim$ 0.5 Ma, respectively. Together with similar hydroclimatic phenomena over corresponding glacial cycles, the two groups of hydrologic and biogeochemical events appear to have been driven largely by oceanographic changes in the Southern Ocean. Therefore, we interpret that the long-term biogeochemical processes originating from the Southern Ocean must have played a crucial role in Quaternary ice-sheet waxing and waning.

Keywords: carbon cycle, long-eccentricity, South China Sea, Quaternary, long-term processes

State Key Laboratory of Marine Geology, Tongji University, Shanghai 200092, China

***Corresponding author.** E-mail: pxwang@tongji.edu.cn

Received 13 September 2013; **Revised** 13 October 2013; **Accepted** 14 October 2013

INTRODUCTION

The South China Sea (SCS), with a total area of 3.5 million km^2 and the maximum depth of 5500 m, is among the largest marginal seas in the world. It offers a special attraction for the Earth sciences, because of its location between the largest continent (Asia) and largest ocean (the Pacific), and its well-preserved hemipelagic sediments. Among the major western Pacific marginal seas, the SCS has the best carbonate preservation because of intensive ventilation of its bottom water [1]. Consequently, the sea provides valuable archives for Late Cenozoic Paleoceanography, especially some of the best-preserved Quaternary sections in the western Pacific, a region that generally has poor carbonate preservation owing to sluggish bottom water.

Over the past 20 yr, the SCS has become a focus of paleomonsoon and paleoceanographic research, culminating with Ocean Drilling Program (ODP) Leg 184 in 1999, targeting East Asian monsoon history with continuous deep-sea records at five drilling sites (Fig. 1) [2]. One of the merits of ODP Leg 184 drilling in the SCS is the finding of long-term changes in the oceanic carbon reservoir at the

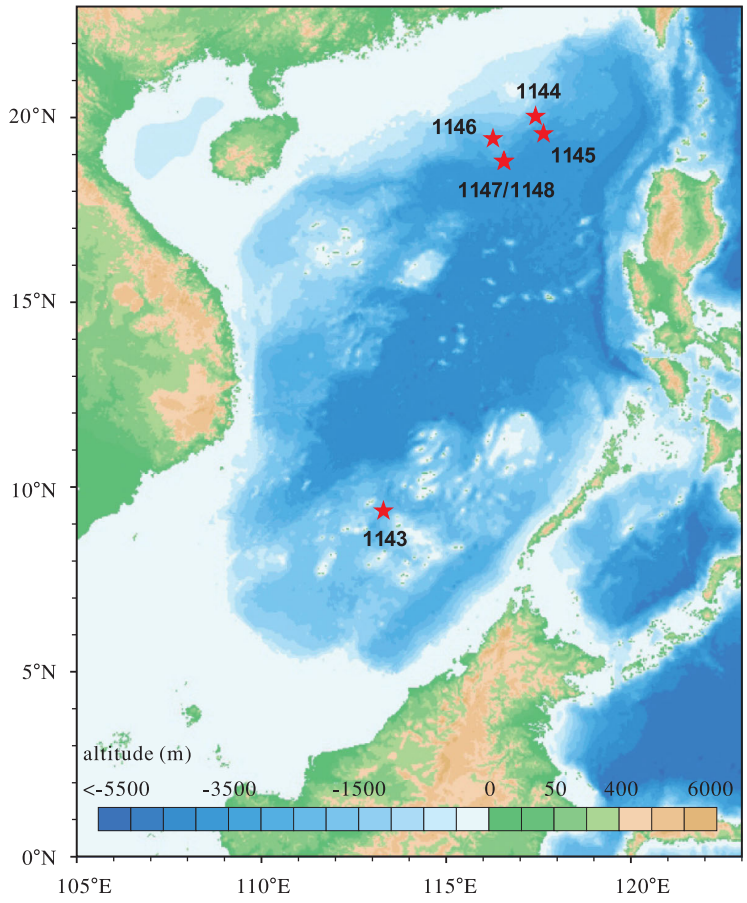

Figure 1. Topography of the SCS with locations of ODP Leg 184 drilling sites [2].

10^5-yr time scale. The δ^{13}C curve is divided by a series of δ^{13}C maxima (δ^{13}Cmax), denoting heavy values over 400–500 kyr cycles. These δ^{13}Cmax events can be correlated globally, and the last 1.6 Myr of the Pleistocene can be divided into three major stages from a carbon perspective (Fig. 2) [3,4]. The SCS finding of long-term changes in the oceanic carbon reservoir and their connection with environmental variation have stimulated further discussions and research [5–7], albeit their driving mechanisms remain unclear. Even the cyclic nature of the long-term variations in δ^{13}C is debatable, since the repeated occurrences of δ^{13}Cmax may be considered just 'nodes' in δ^{13}C fluctuations [8].

The present paper is a review of recent progress in paleoceanography of the SCS and worldwide implications of long-term cycles in the oceanic carbon reservoir. We will show that the long-eccentricity cycles are inherent in the Earth system and have been functioning in the oceanic carbon system at least across the Cenozoic, but modified in the Quaternary, probably in response to the development of polar ice sheets. These long-term cyclic changes in turn have profoundly influenced the global environmental evolution by causing long-term changes across glacial cycles. It is believed that individual interglacials are different not only because of their specific orbital parameters at a particular time, but also because of their inducement of long-term processes that persist over several glacial cycles.

LONG-TERM CYCLES IN OCEAN RECORDS

Long-term rhythms of 10^5 yr are not new to Quaternary science. Long cycles across several glacial/interglacial alterations were noticed in Pacific deep-sea $CaCO_3$% curves from the Albatross expedition some 60 yr ago [10], and a 500-kyr periodicity in winter temperature reconstructions from the tropical Atlantic was detected by micropaleontologists ∼40 yr ago [11]. Since then, similar long periodicities have been identified in tropical carbonate records [12,13] and in Quaternary δ^{13}C records [14–17]. Long-term cycles have also been recognized in terrestrial records, specifically from the Loess Plateau in China [18,19]. However, most Quaternary long-term cycles varied greatly in duration and in assumed formation mechanism until recent years, when long-term, high-resolution records became available from the deep ocean. By contrast, all long-term cycles reported from the pre-Quaternary ocean have been paced at ∼400-kyr rhythm and ascribed to the long-eccentricity in orbital forcing.

Long-term cycles in carbon reservoir of the pre-Quaternary ocean

ODP Leg 184 has established a high-resolution sequence for the entire Neogene at ODP Site 1148 (18°50′N, 116°34′E, water depth 3294 m), which provides the best Neogene deep-sea archive in the western Pacific region [3,20]. Detailed analyses show that the 400-kyr long-eccentricity cycles are pervasive throughout the Neogene, although their strengths varied with time. The long-eccentricity cycle in the SCS was first presented in the K/Al ratio record as a proxy of chemical weathering in the late Pliocene at ODP Site 1145 (19°35′N, 117°38′9E, water depth 3175 m) [21]. This was recently confirmed by new data from ODP Site 1143, showing K/Al ratio responses to the long-eccentricity throughout the last 5 Myr [22].

Nonetheless, the long-eccentricity signal can be observed much more extensively in marine carbon isotope records, as seen from a compilation of δ^{13}C records from the global ocean over the last 5 Myr. In Fig. 3, all the records show δ^{13}Cmax at eccentricity minima during the Pliocene, although this relationship became obscured in the Pleistocene after ∼1.6 Ma. This result is convincing, since the time

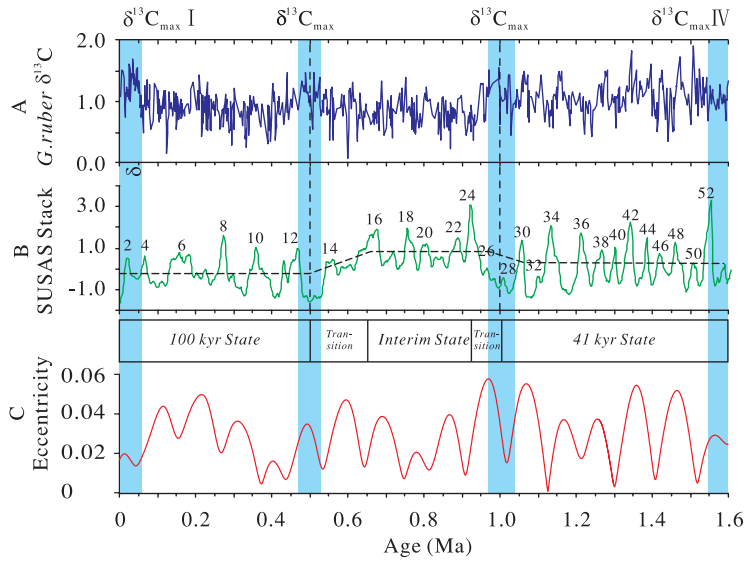

Figure 2. Three major stages of the last 1.6 Myr in a carbon perspective. (A) Triple division based on δ^{13}Cmax events, represented by planktonic δ^{13}C of ODP Site 1143, southern SCS (9°22′N, 113°17′E; water depth 2772 m). (B) Tripledivision into '100-kyr state', 'interim state', and '41-kyr state' based on Subtropical South Atlantic Susceptibility (SUSAS) stack from Schmieder *et al.* [9]. (C) Eccentricity (modified from [4]).

series used for the comparison includes both benthic and planktonic records, and covers open and marginal basins from the Atlantic and Pacific [7].

The 400-kyr cyclicity in δ^{13}C is characteristic of the entire Neogene archive from the SCS, with δ^{13}C records of the early to middle Miocene representing the best example. Fig. 4 shows a 4-Myr record of benthic foraminiferal δ^{13}C in the middle Miocene (16.5 Ma through 12.5 Ma) from ODP Site 1146 (19°27′N, 116°16′E., water depth 2092 m), with long-term cycles all corresponding to the long-eccentricity periodicity (Fig. 4A,B) [23], although the correspondence is not perfect. Individual long-term cycles of δ^{13}C may slightly differ in duration but average 400 kyr, just like the 100-kyr glacial cycles in the Late Pleistocene ranging from 80 to 120 kyr. The long-eccentricity forcing of δ^{13}C ceased after 13.9 Ma (Fig. 4B), presumably in response to the amplification of the Antarctic ice sheet [23,25], a mechanism explored below.

Importance of the long-eccentricity has become generally acknowledged, since it also occurs in high-resolution stratigraphic sections from longer and deeper geologic time. Among the orbital parameters, the 400-kyr long-eccentricity cycle remains stable in duration throughout the geologic history; hence, it is the best rhythm for use in astronomical stratigraphy [26]. In orbital forcing, eccentricity enters the climate system by modulating the amplitude of climatic precession. However, the 400-kyr cycles are best recorded in marine δ^{13}C and carbonate records. This can be explained by the long residence time of carbon, of the order of 10^5 yr in the oceanic reservoir, which amplifies lower frequency or dampens higher frequency orbital variations of the ocean carbon cycle [27,28].

Intriguingly, long-eccentricity forcing was recognized three decades ago by sedimentologists in carbonate sequences in Italy [29–31] and the Pacific [32], later supported by extensive lithological and isotopic evidence [33,34]. Now the 400-kyr cycles form the basis of astronomical calibration in stratigraphy of the Cretaceous [35,36], following successful application to the Cenozoic. In the Cenozoic, high-resolution analyses of deep-sea cyclic sedimentary successions of the Paleogene reveal even more pronounced long-eccentricity cycles [28,37]. For the Paleocene epoch, 24 long-eccentricity cycles have been uncovered based on XRF (X-ray Fluorescence) core scanning and magnetic susceptibility measurements [38] and, as follow-up, an astronomically calibrated time scale for the early Paleogene (47–65 Ma) has been proposed (Fig. 4C–E) [39].

Long-eccentricity cycles have been widely observed in marine sections, such as in δ^{13}C records of the late Paleocene–early Eocene [27], and in lithological bundles of the early Paleocene in Spain [40]. The 400-kyr long-eccentricity is so remarkable in the deep-sea Oligocene sequence that it has been termed the 'heartbeat' of the ocean system for the Oligocene (Fig. 5A–B) [28,41–43]. A new and encouraging trend is emerging to connect the astronomical and sequence stratigraphy, with the fourth order of sea level changes in the Mesozoic and Cenozoic likely corresponding to the 400-kyr long-eccentricity [44]. If confirmed, the long-eccentricity will be not only the heartbeat of Earth's climate evolution, but also a 'tuning fork' in geologic time measurement.

Long-term cycles in carbon reservoir of the Quaternary ocean

The above review of long-term cycles raises a logical question: Why did the long eccentricity cycles disappear in the Quaternary? As displayed in Fig. 3, all δ^{13}C time series display clear 400-kyr cycles in the Pliocene part, and a total of 13 long-term δ^{13}Cmax events corresponding to long eccentricity minima can be recognized in the last 5 Ma (Table 1) [7]. However, the rhythmic occurrence of δ^{13}Cmax at long-eccentricity minimum ended at 1.6 Ma. Second, the later δ^{13}Cmax events are out of phase with the eccentricity signal, with the interval between δ^{13}Cmax extending to 500-kyr in the last million years (Fig. 3; Table 1).

As shown by spectral analyses, the 400-kyr long-eccentricity signal in δ^{13}C records is obscured after

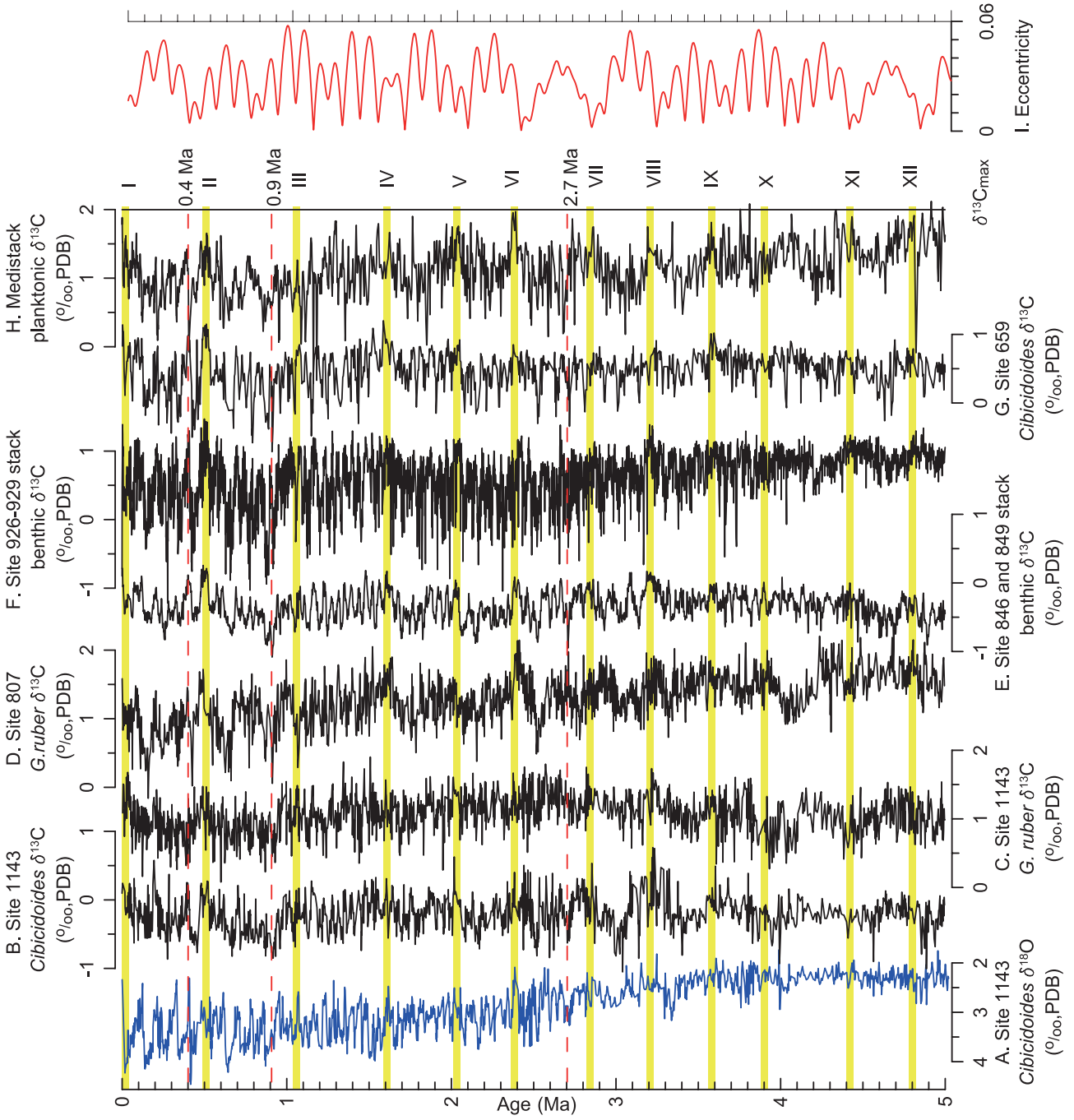

Figure 3. Carbon isotopic records from the SCS and global ocean over the past 5 Myr. A–C. ODP Site 1143, South China Sea: (A) benthic $\delta^{18}O$; (B) benthic $\delta^{13}C$; (C) $\delta^{13}C$. (D and E) Pacific: (D) planktonic $\delta^{13}C$ of ODP Site 807; (E) stacked benthic $\delta^{13}C$ of ODP Sites 846 and 849. (F and G) Atlantic: (F) stacked benthic $\delta^{13}C$ of ODP Leg 154 (Sites 926–929); (G) benthic $\delta^{13}C$ of ODP Site 659. (H) Mediterranean: stacked planktonic $\delta^{13}C$ (based on [7,22]). Yellow bars indicate $\delta^{13}C$max; red dotted lines denote major events of ice-sheet development at 2.7, 0.9 and 0.4 Ma.

1.6 Ma at all open-ocean sites but not in the Mediterranean Sea which has been largely isolated from the global ocean since the late Miocene (Fig. 3H). Accordingly, the obscuration of the 400-kyr cyclicity since 1.6 Ma can be attributed to the restructuring of the global ocean, which disturbed the response of the oceanic carbon reservoir to the long eccentricity, as discussed in the following section. Here, we emphasize that the long-eccentricity signal remains clear in climate proxy sequences, such as the K/Al ratio representing intensity changes of chemical weathering. Data from the SCS show the K/Al ratio responses to the long eccentricity throughout the 5 Myr [22].

As seen in Fig. 1, the Pleistocene record is punctuated by four $\delta^{13}C$max events: $\delta^{13}C_{max\text{-}I}$,

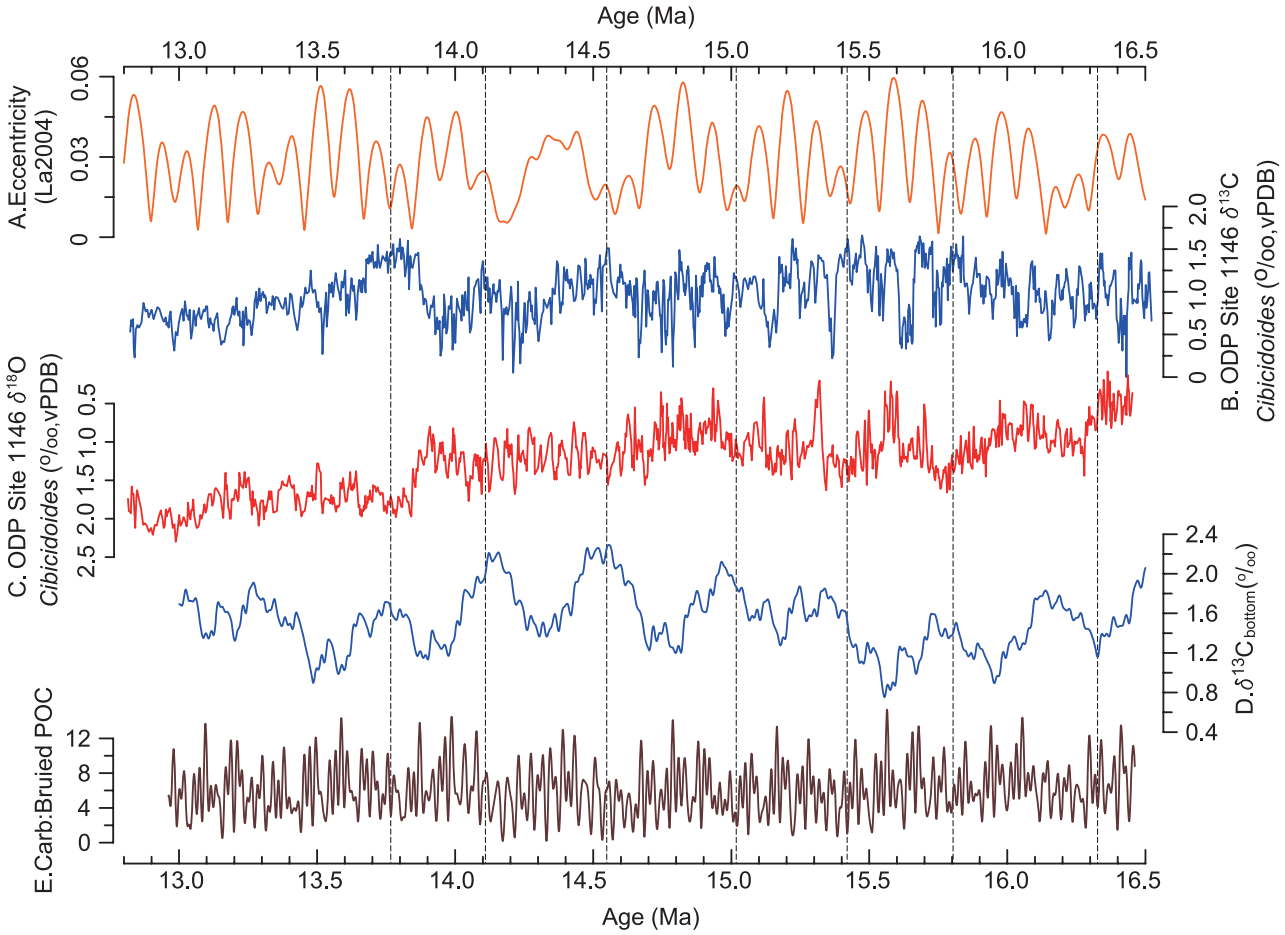

Figure 4. 400-kyr long-eccentricity cycles in the middle Miocene records from ODP Site 1146, northern SCS, with data-model comparison. (A) Eccentricity cycles; (B) benthic $\delta^{13}C$; (C) benthic $\delta^{18}O$ (modified from [23]). (D) numerical simulation of average $\delta^{13}C$ in bottom water; (E) modeled burial ratio of total $CaCO_3$ to POC (modified from [24]). Dotted vertical lines denote $\delta^{13}C$ max occurring at the long-eccentricity minima.

which began in marine isotope stage (MIS) 3 around 50–60 kyr ago; $\delta^{13}C_{max\text{-}II}$ (MIS 13, 0.47–0.53 Ma); $\delta^{13}C_{max\text{-}III}$ (MIS 27–29, 0.97–1.04 Ma); and $\delta^{13}C_{max\text{-}VI}$ (MIS 53–57, 1.55–1.65 Ma). Since the same cyclicity is also found in carbonate curves, the δ^{13}Cmax events must signify major reorganization in the carbon reservoir of the global ocean, which might have triggered major changes in glacial cyclicity [3,4]. In a search for the possible causal relationship between the major events in the evolution of the global ice sheets and the oceanic carbon reservoir, both physical and biological aspects of the environmental evolution of the Quaternary ocean must be examined.

MAJOR EVENTS IN ENVIRONMENTAL EVOLUTION OF THE QUATERNARY OCEAN

Recent years have seen major leaps in the knowledge of the environmental evolution in the Quaternary, largely from deep-sea, ice-core and speleothem records. Not only have the glacial/interglacial cycles been identified, long-term processes beyond glacial cycles have also attracted research interest. A number of major steps across glacial cycles have been recognized in records of both ice-sheet development and oceanic carbon reservoirs. All these steps are well represented in the SCS, as demonstrated here based on $\delta^{18}O$ and $\delta^{13}C$ curves at ODP Site 1143 in the southern SCS (Fig. 6). Like many other similar records, the $\delta^{18}O$ curve is marked by the establishment of the Northern Hemisphere ice sheet at 2.7 Ma, the mid-Pleistocene transition (MPT) from 40-kyr cycles to 100-kyr cycles centered on 0.9 Ma and the mid-Brunhes event (MBE) centered on 0.4 Ma with a significant increase of fluctuation amplitude in glacial cycles. The $\delta^{13}C$ curve is divided by a series of δ^{13}Cmax, representing heavy values over 400–500-kyr cycles. As discussed above, before 1.6 Ma the occurrence of δ^{13}Cmax closely followed the long-eccentricity minimum, but after 1.6 Ma the

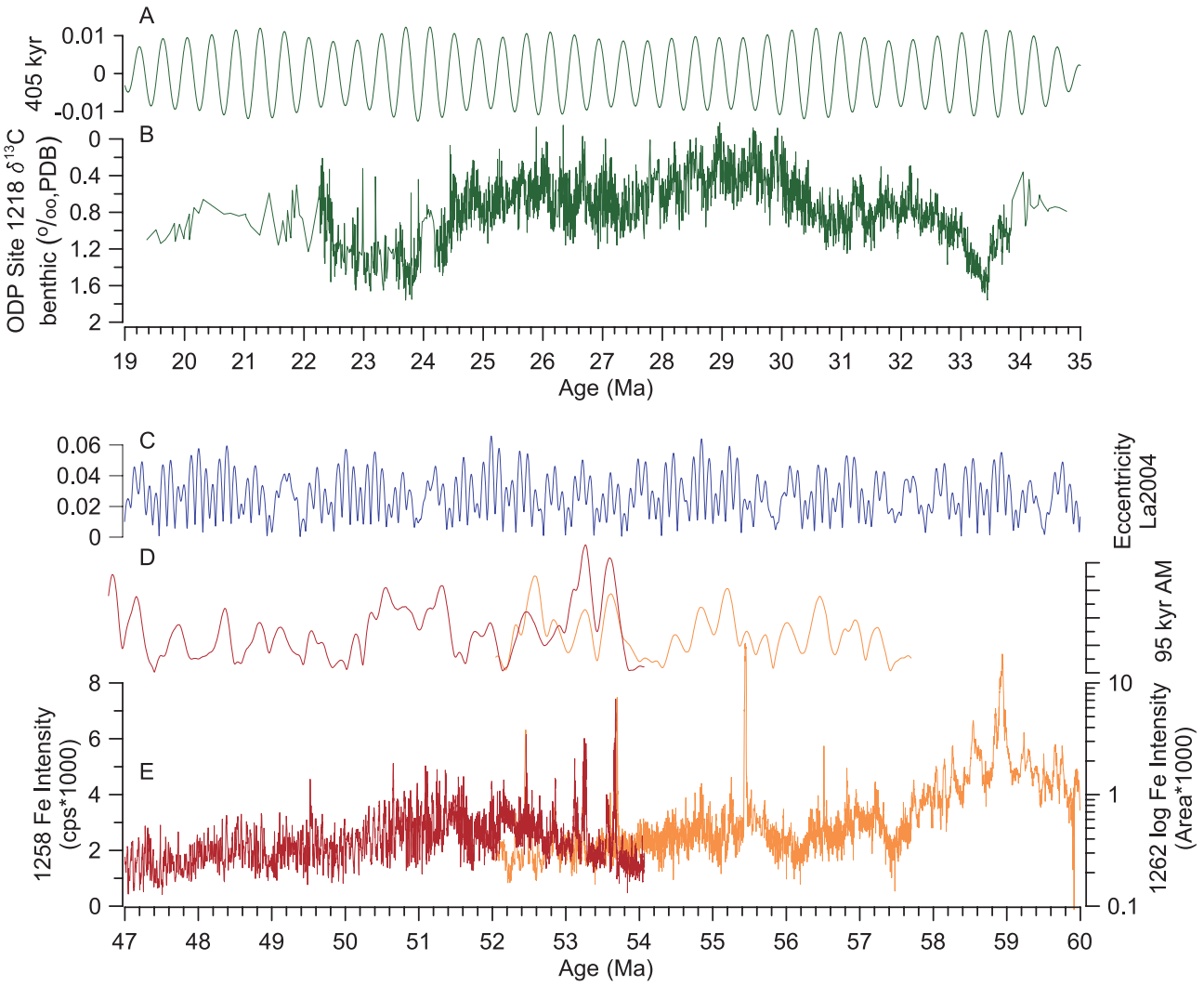

Figure 5. Long-eccentricity in the Paleogene records. Upper: carbon isotope in the Oligocene. (A) Long eccentricity; (B) benthic δ^{13}C from ODP Site 1218, equatorial Pacific [37]. Lower: Fe content in the early Paleogene. (C) Eccentricity; (D) 95-kyr amplitude modulation showing 405-kyr cycles; (E) Fe intensity based on XRF core scanning. ODP Sites 1258 in red and 1262 in orange [39].

cyclicity was disturbed, likely associated with reorganizations of the oceanic carbon reservoir. It has been postulated that the mode shift in glacial cycles at the MPT and MBE was genetically related to corresponding δ^{13}Cmax events [3,4]. All these events are discussed in the following sections in chronological order.

From the 2.7 Ma event to 1.6 Ma event

(i) *Restructuring of the Global Ocean.* The supreme feature of the Plio-Pleistocene turn is marked by the initiation of major Northern Hemisphere glaciation and the establishment of a glaciation or 'glacial cycles' regime in the climate and ocean systems. In the context of gradual Cenozoic cooling, milestones in climate evolution occurred at ∼2.7 and ∼1.6 Ma. The 2.7 Ma event was the onset of extensive Northern Hemisphere glaciation and beginning of 40-kyr obliquity glacial cycles [45–47], and the 1.6 Ma event indicated a reorganization of the oceanic carbon reservoir that obscured its response to the 400-kyr long-eccentricity forcing [7]. In the SCS, the 2.7 and 1.6 Ma events can be recognized in both the δ^{18}O (Fig. 3A) and δ^{13}C records (Fig. 3B and C).

Although the orbital forcing of glaciation is generally accepted, the triggering and forcing mechanism of these events remains a subject for further research. Some recent studies emphasize the significance of ocean stratification and the central role played by the Southern Ocean. That is because this stratified ocean controls carbon exchange between the atmosphere and ocean on glacial cycles, by serving as a lid on a

Table 1. Comparison between carbon isotope maximum events and eccentricity minima over the last 5 Myr [7]

Eccentricity minimum No.	Age (Ma)	δ^{13}Cmax no.	Age (Ma)	δ^{18}O MIS
1	Present	I	0–0.05	1–3
2	0.40	II	0.47–0.53	13
3	0.80			
		III	0.95–1.00	25–27
4	1.21			
5	1.62	IV	1.55–1.65	53–57
6	2.02	V	2.00–2.06	75–77
7	2.43	VI	2.38–2.44	93–95
8	2.83	VII	2.73–2.80	G7–G9
9	3.24	VIII	3.20–3.29	KM5-M1
10	3.64	IX	3.56–3.61	Gi1
11	4.04	X	3.97–4.01	Gi20
12	4.44	XI	4.39–4.42	CN6
13	4.85	XII	4.75–4.82	NS6-Si2

larger volume of the deep ocean. Therefore, it is crucial to uncover how the chemical divide formed between Antarctic deep water and Subantarctic intermediate water [48]. Comparison of oceanic benthic δ^{13}C from various basins and water depths may provide a clue to answering this question. In the Southern Ocean, benthic δ^{13}C records from intermediate water (ODP Site 1088, water depth 2082 m) and deep water (ODP Site 1090, water depth 3702 m) are similar for the period 6.3 through 2.7 Ma. However, their carbon isotope values begin to diverge at 2.7 Ma, marked by abrupt decrease of δ^{13}C at Site 1090 relative to Site 1088 (Fig. 7, upper panel) [49]. It has been proposed that global cooling that caused vertical stratification in the southern and northern polar oceans at 2.7 Ma may in turn have increased the quantity of carbon dioxide trapped in the abyss, amplifying the global cooling [50]. Meanwhile, increased summer sea surface temperature (SST) in the western subarctic Pacific, in response to an increase of stratification, may have provided water vapor to build the Northern Hemisphere ice sheets [47].

(ii) *2.7 Ma Event.* The appearance of larger ice sheets and stratification of the polar oceans at 2.7 Ma impacted the entire ocean, including surface and deep-water temperatures. Thus, the obliquity-related component of tropical SST variability not only increased in amplitude ∼2.7 Ma, but became highly coherent between the benthic δ^{18}O and orbital forcing [51]. In the southern SCS, SST began to oscillate strongly since 2.7 Ma, following a steady state at ∼29°C in the Pliocene (Fig. 8A) [52]. In the eastern Pacific, SST contrast between the equator and 32°N increased by ∼2°C around 2.7 Ma, and amplitude of SST variations also drastically increased in response to obliquity forcing at the same time (Fig. 8B) [53]. For the deep ocean, the 2.7 Ma event marks the end of the 'Late Pliocene transition' beginning at 3.0 Ma with a 2°C decrease of average bottom water temperature in the North Atlantic (Fig. 8C) [54].

The 2.7 Ma event also influenced regional monsoon systems. In the modern SCS, primary productivity is controlled by the winter monsoon, with productivity increases driven by an intensified monsoon. As shown by sediment records at ODP Site 1143 in the southern SCS, total organic carbon significantly increased at 2.7 Ma, suggesting the intensification of monsoon activity (Fig. 8H) [56]. Similarly, African monsoons also intensified at 2.7 Ma, as revealed by eolian dust in Atlantic sediments. The strengthened African monsoons switched from a precession band to an obliquity band of variations after 2.7 Ma (Fig. 8K and L) [61,62].

Therefore, the 2.7 Ma event is not only well known to the climate community as marking the onset of major Northern Hemisphere glaciation, it was also found to have been accompanied by significant reorganization of the ocean structure. Around 2.7 Ma, stratification of the polar water column led to a drastic decrease of biogenic opal in the subarctic Pacific sediments (Fig. 8I) [59], and a thermal division between deep and intermediate waters in the Southern Ocean isolated its abyss to become the largest carbon reservoir of the global ocean [48]. The appearance of meridional SST contrast in the eastern Pacific ended the uniform Pliocene pattern of SST across the tropical Pacific [53]. Importantly, all trends of oceanographic change were not limited to the 2.7 Ma event, since their sequential development had given rise to the next event at 1.6 Ma.

(iii) *1.6 Ma Event.* Remarkable in its sequential development is the further depletion of the deep-water δ^{13}C in the Southern Ocean, which became even lighter after 1.6 Ma than that of the Pacific (Fig. 7, lower panel) [49], especially during glacial periods [63]. All these observations testify to the further isolation of the deep Southern Ocean. At the same time, deep-water δ^{13}C in the North Atlantic also decreased and diverged from its intermediate

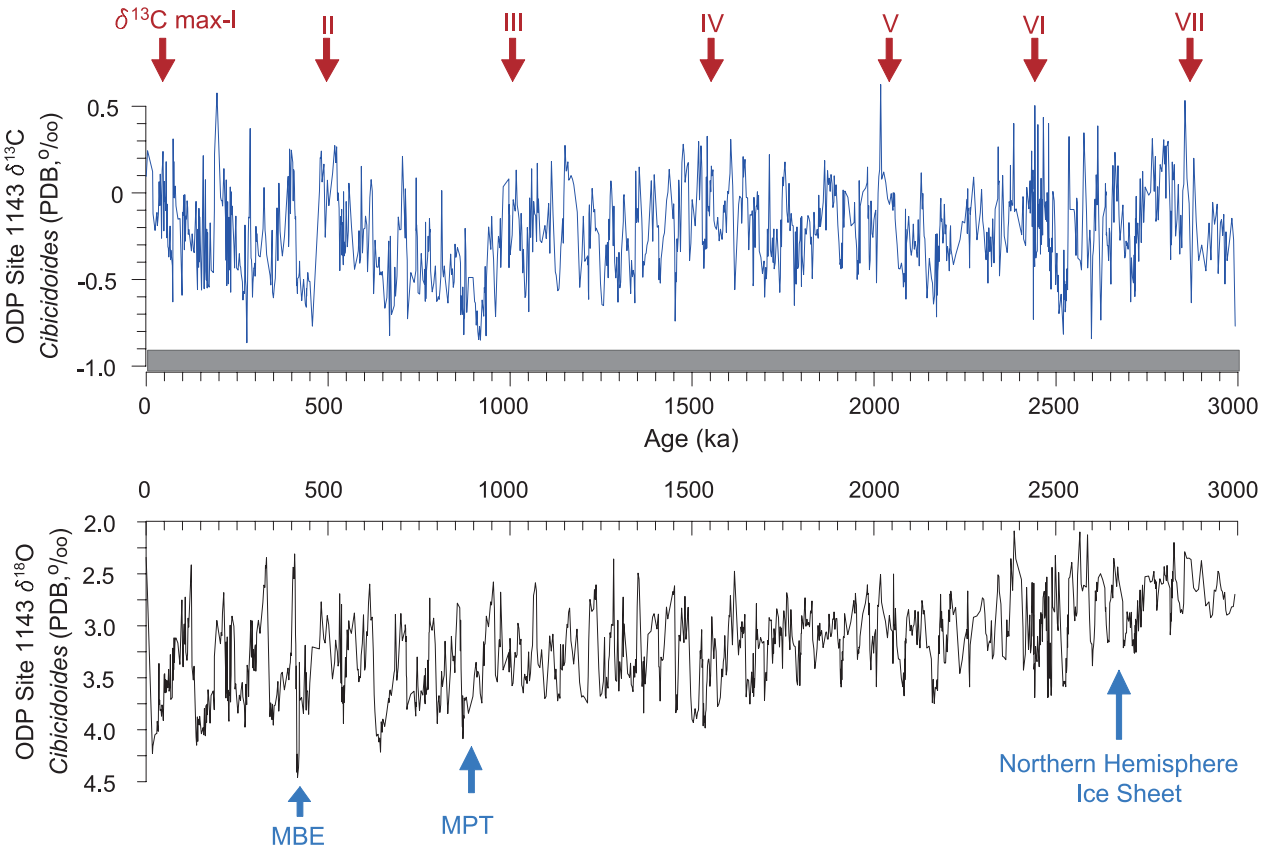

Figure 6. Major events shown in isotope records of ODP Site 1143, SCS. Upper curve: benthic $\delta^{13}C$; lower curve: benthic $\delta^{18}O$. Red arrows: carbon isotope maxima; blue arrows: ice-sheet development. MPT: mid-Pleistocene transition; MBE: mid-Brunhes event.

water counterpart (Fig. 7, lower panel), suggesting the intensification of the chemical divide in the Atlantic between well-ventilated intermediate water and poorly ventilated deep water [49].

Across the equatorial Pacific, the modern asymmetric pattern of the SST distribution first took shape around 1.6 Ma. Both the Mg/Ca paleo-SST difference (Fig. 8D) [55] and $\delta^{18}O$ gradient [64] between the West and East Pacific abruptly strengthened at 1.6 Ma, indicating the formation of a cold tongue in the East and emergence of East–West asymmetry [65,66]. Therefore, the 1.6 Ma event represents a further step in the restructuring of the global ocean, from the Pliocene toward the Pleistocene pattern.

Like its 2.7 Ma counterpart, the 1.6 Ma event also generated clear biological and geochemical response of the global ocean. In the SCS, total organic carbon and alkenone concentration declined at 1.6 Ma (Fig. 8E and H), suggesting a sharp reduction in productivity [56]. The same event was widely observed in the open Pacific Ocean, following the 'late Pliocene/early Pleistocene productivity maximum'in the East Pacific, lasting from 3.0 to 1.6 Ma (Fig. 8F) [57]. In terms of diatom production, 1.6 Ma witnessed a depression of biogenic opal accumulation in the subtropical Atlantic (Fig. 8J) [60], while a high opal accumulation stage in the Southern Ocean started around that time [67,68]. This was also a period with low eolian dust input in Atlantic sediments, implying the weakening of the African monsoons (Fig. 8K and L).

In summary, 2.7 and 1.6 Ma were two major steps in restructuring the global ocean into the glacial regime. Under the background of the late Neogene cooling, the ocean separated into an actively circulating portion and sluggish abyss in the Southern Ocean, and the zonal SST asymmetry formed more clearly in the equatorial Pacific. Since the restructuring of the ocean was in conjunction with the growth of polar ice sheets, it must have influenced the response of glacial and oceanic carbon cycles to the orbital forcing. An important feature of the 1.6 Ma event is the obscuration of the 400-kyr long-eccentricity signal in the marine $\delta^{13}C$ records. Before 1.6 Ma, $\delta^{13}C$max occurred at eccentricity minima leading to 400-kyr cycles in $\delta^{13}C$ records, but this relationship became obscured at 1.6 Ma when

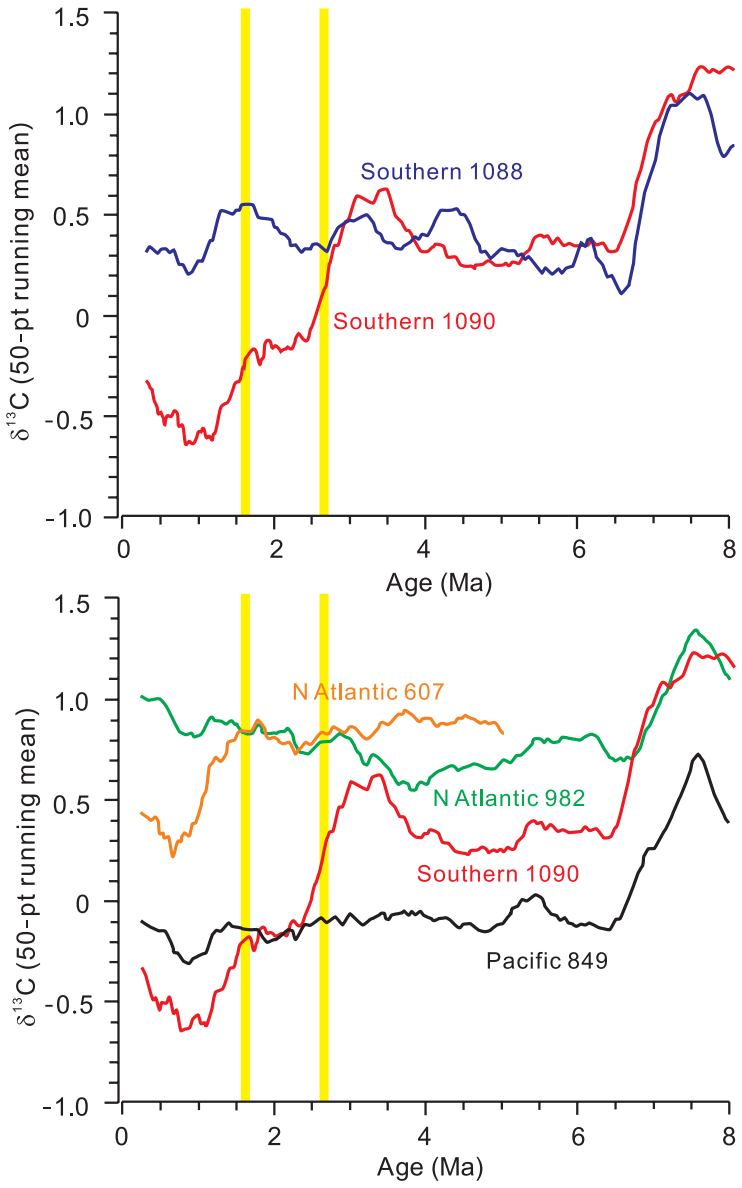

Figure 7. Benthic $\delta^{13}C$ records in 50-pt running mean over the past 8 Myr. Southern Ocean: ODP Site 1090 (water depth 3702 m), ODP Site 1088 (water depth 2082 m); North Atlantic: ODP Site 607 (water depth 3400 m), ODP Site 982 (water depth 1100 m); East Pacific: ODP Site 849 (water depth 3850 m) [49]. Yellow bars denote major events occurred at 2.7 and 1.6 Ma, respectively.

the ocean was restructured into a more typical glacial regime (Fig. 3)[7]. The change in the oceanic carbon reservoir is believed to be associated with the formation of the large deep-water carbon pool in the Southern Ocean, as discussed below.

The 1.6 Ma event affected not only the long (400-kyr) but also the short (100-kyr) eccentricity-related signals. Before 1.6 Ma, $\delta^{18}O$ and $\delta^{13}C$ were basically in phase with eccentricity in both the 400- and 100-kyr bands, whereas during the Pleistocene, $\delta^{18}O$ and $\delta^{13}C$ became anti-phase in the 100-kyr band [7]. Moreover, cross-spectral relationships between the LR04 benthic stack and 21 June insolation at 65°N reveal the essential establishment of $\delta^{18}O$ coherence with the precession components of insolation at 1.6 Ma, after a very unstable stage between 3.0 and 1.6 Ma [69]. From analyzing Atlantic paleoclimate records, Rutherford and D'Hondt [70] found strengthening semiprecession cycles of the tropical origin in the Northern Hemisphere around 1.5 Ma ago. Their subsequent propagation to higher latitudes triggered a transition to sustained 100-kyr glacial cycles. All these findings hint at an enhanced role for low-latitude processes in the global ocean, probably linked with the emergence of the new thermal pattern in the equatorial Pacific after 1.6 Ma.

Carbon isotope maximum-III and mid-Pleistocene transition

The MPT and MBE are the most important turning points in the environmental evolution of the last million years. The MPT (sometimes called 'mid-Pleistocene revolution') is used to denote intensification and prolongation of the glacial/interglacial cycles from 41- to 100-kyr frequencies (Fig. 6). The MPT is currently considered a long-duration process from 1.25 to 0.7 Ma, centered at 0.9 Ma [71]. Since glacial cycles are central to Quaternary studies, the MPT has attracted increasing attention in the paleoclimate community. In the SCS, the MPT interval at ODP Site 1144 with the highest Pleistocene sedimentation rate in the basin has been subjected to high-resolution analyses [72–74]. In only the last five years, numerous publications have reviewed the MPT or explored its origin [54,75–79], mostly with a focus on physical aspects such as ice-sheet size, temperature, or frequency or phase changes of the cycles.

On the other hand, an increasing number of biological and biogeochemical events in the last million years have been recently discovered, including diatom blooms in oligotrophic oceans [80–82], proliferation of coccolithophores [80,83] and long-term changes of $\delta^{13}C$ or $\delta^{13}C$max events [3,4,8]. Köhler and Bintanja [5] used numerical modeling to show that deep-ocean $\delta^{13}C$ must have responded differently to forcing in the Southern Ocean prior to and after the MPT. It remains uncertain, however, whether there is any connection between the biological/biogeochemical events and physical events of the ice sheets, and whether these discrete events are at all related to each other.

The crucial turning point of the MPT occurred at the onset of MIS 22 (0.9 Ma) when the global ice sheets increased rapidly in size [78], but the cooling process began well before the MPT. In the SCS, glacial $U^{k'}_{37}$ SST remarkably decreased by 2°C

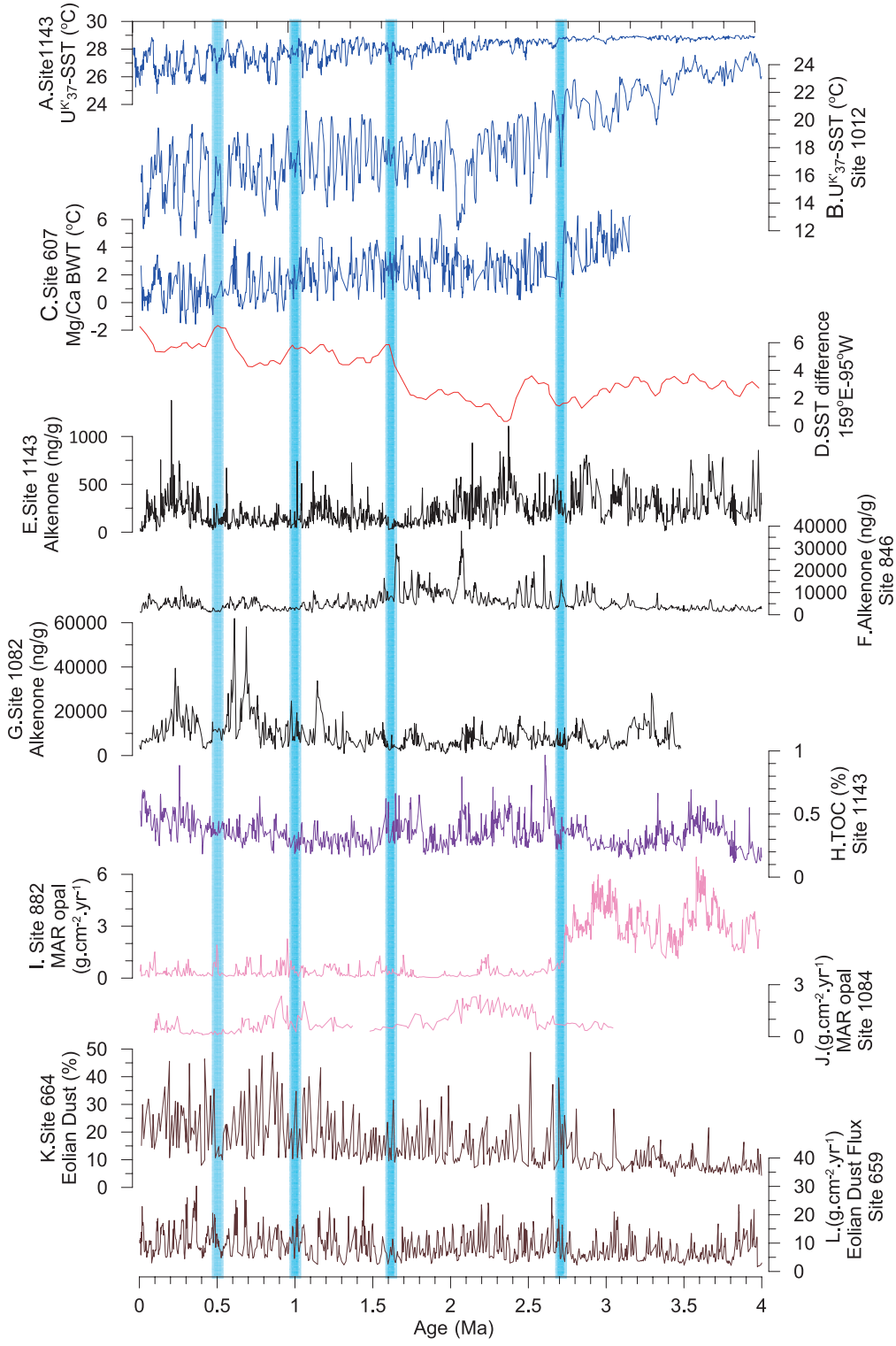

Figure 8. Paleoclimate and biogeochemical records over the past 4 Myr from various site localities. (A) $U^{k'}_{37}$-based SST, ODP Site 1143, SCS [52]; (B.) $U^{k'}_{37}$-based SST, ODP Site 1012, East Pacific [53]; (C) Mg/Ca bottom water temperature, ODP Site 667, Atlantic [54]; (D) zonal SST gradient between 159°E and 95°W, equatorial Pacific [55]; (E) alkenone concentration (ng/g), ODP Site 1143, SCS [56]; (F) alkenone concentration (ng/g), ODP Site 846, Eastern Pacific [57]; (G) alkenone concentration (ng/g), ODP Site 1082, South Atlantic [58]; (H) total organic carbon%, ODP Site 1143, SCS [56]; (I) MAR of opal (g cm^{-2} kyr^{-1}), ODP Site 882, North Pacific [59]; (J) MAR of opal (g cm^{-2} kyr^{-1}), ODP Site 1084, South Atlantic [60]; (K) eolian dust (%), ODP Site 664, off West Africa [61]; (L) Eolian dust flux (g cm^{-2} yr^{-1}), ODP Site 659, off West Africa [62]. Blue bars denote major events occurred at 0.5, 1.0, 1.6 and 2.7 Ma.

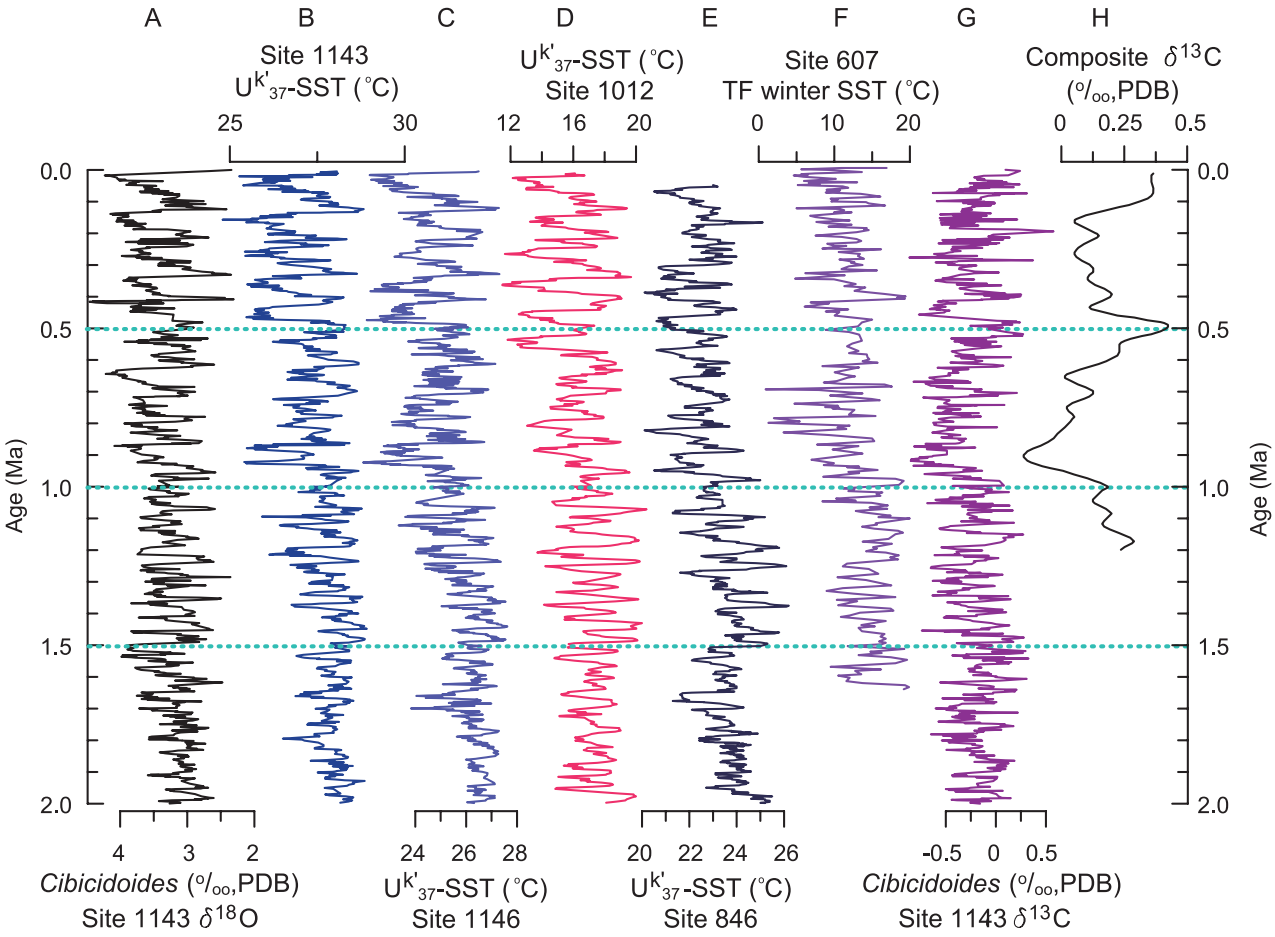

Figure 9. SST over the last 2 million years. (A) Benthic $\delta^{18}O$ at ODP Site 1143, SCS, for correlation; (B) $U_{37}^{k'}$-based SST at ODP Site 1143, SCS; (C) $U_{37}^{k'}$-based SST at ODP Site 1146, SCS [51]; (D.) $U_{37}^{k'}$-based SST at ODP 1012, East Pacific [53]; (E) $U_{37}^{k'}$-based SST at ODP 846, East Pacific [57]; (F) transfer-function-based winter SST at ODP 607, North Atlantic [15]; (G) Benthic $\delta^{13}C$ at ODP Site 1143, SCS [3]; (H) smoothed composite benthic $\delta^{13}C$ [8].

from ∼1.5 to ∼1.1 Ma (Fig. 9B and C) [51,52] until a rapid warming at MIS 31, which was reflected in the South Pole region by the collapse of the West Antarctic ice sheet [84]. MIS 31 was an abnormally warm and long interglacial period (1.085–1.055 Ma) with possibly a 2–5°C SST rise, and the retreat of ice cover gave rise to phytoplankton blooms [85]. The trend of enhanced productivity continued to the next interglacial, as evidenced by the occurrence of laminated diatom ooze during MIS 29 in the Southern Ocean [86]. In the SCS, the abundance of small-sized coccoliths *Gephyrocapsa* spp. formed a large spike at MIS 31, followed by a drastic increase in abundance from MIS 29 to MIS 25 (Fig. 10) [87].

This warm and productive period of MIS 29–25 covers the carbon isotope episode $\delta^{13}C_{max\text{-}III}$ (Figs 2 and 3) [4], but afterward the benthic carbon isotope drastically declined by 0.35‰ or even 1‰ from MIS 25 to MIS 22, attaining the lowest value of the last 5 Myr [8,78]. The negative shift of $\delta^{13}C$ was accompanied by 2–3°C SST cooling in the SCS [52] and in the global ocean [79] (Fig. 9), and a significant sea level lowering caused by ice-sheet expansion. It was only during MIS 22 when Antarctic ice volume abruptly increased to withstand melting, and the glacial cycle prolonged to 100 kyr [78].

After the 0.9-Ma event, $\delta^{13}C$ again shows a general increase toward the next $\delta^{13}C$max (Fig. 3). Noteworthy is the striking similarity between $\delta^{13}C$ and SST; the two curves are nearly parallel from 2.0 to 0.5 Ma (Fig. 9G and H), implying some common driving mechanism. A further step toward the modern global ocean pattern is that the zonal gradient of SST in the eastern equatorial Pacific reached modern values by 0.9 Ma [89]. The close connection between the changes of $\delta^{13}C$ and SST is self-evident, but its mechanism requires further scrutiny. As discussed in the 'Hypothetical interactions between physical and biogeochemical processes' section, we attribute the long-term changes of both $\delta^{13}C$ and SST to biological processes in the ocean.

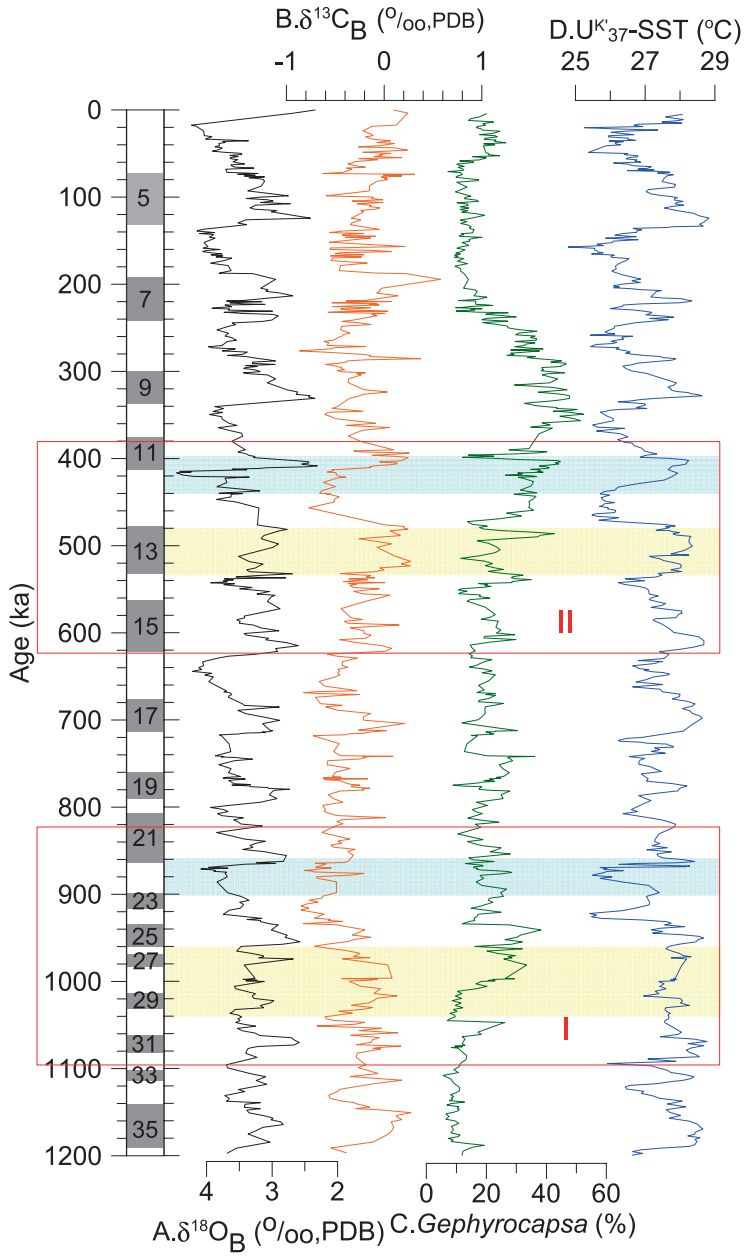

Figure 10. Late Pleistocene major events recorded at ODP Site 1143, southern SCS. (A) benthic $\delta^{18}O$ [88]; (B) benthic $\delta^{13}C$ [3]; (C) small coccoliths of *Gephyrocapsa* [87]; (D) $U_{37}^{k'}$-based SST [52]. Red boxes represent two groups of events: I $\delta^{13}C_{max\text{-}III}$/MPT, II $\delta^{13}C_{max\text{-}II}$/MBE; yellow bars denote $\delta^{13}C_{max\text{-}II}$ events; blue bars denote MPT and MBE, respectively.

Carbon isotope maximum-II and mid-Brunhes event

The MBE was first discovered in the 1980s within Atlantic deep-sea records, as a climate shift and carbonate dissolution event around 0.4 Ma [90–92]. MBE importance was highlighted after observing that in Antarctic ice cores variations of temperature and CO_2 concentration in glacial cycles abruptly increased after the MBE [93]. Like the MPT, the MBE is now considered a critical period of transition to enhanced amplitudes of glacial/interglacial cycles, centered on MIS 11 (~0.4 Ma). As another active area of Quaternary environmental research, the MBE has been the subject of many recent review papers [94–96].

As with the MPT, the MBE was prefaced by a warming and productive episode, this time in MIS 15–13, again most prominently in the Antarctic region. MIS 15–13 was a time of climatic anomaly in the Southern Ocean with characteristics of a single, prolonged interglacial period characterized by unusual depositional features, indicative of collapse of the West Antarctic ice sheet [97]. In the Pacific sector of the Southern Ocean, diatom sedimentation suddenly increased from 0.62 Ma (MIS 15) to MIS 13, with the increase of biogenic opal proportion (%) by a factor of nearly 10 (Fig. 11B) [82]. This precipitous change was presumably associated with melting of the West Antarctic ice sheet, which resulted in biogenic blooms in open waters. Since the Southern Ocean is diverse with specific regional features, however, biogenic blooms did not occur in its Atlantic sector, where instead the 'lukewarm interglacials' of MIS 15 and 13 had relatively low productivity [98].

Of particular interest is glacial stage MIS 14. Not only did its diatom productivity remain as high as in interglacials MIS 13 and 15 (Fig. 11B), the discovery of thick, laminated, near-monospecific diatom ooze layers in the southern Atlantic in MIS 14 also suggests an Antarctic influence in the subtropical oligotrophic ocean (Fig. 11D) [81,100,101]. Although no causal link has been established, this abnormal glacial MIS 14 was immediately followed in MIS 13 by the carbon isotope episode $\delta^{13}C_{max\text{-}II}$ [4]. Following the MIS 13 peak, benthic $\delta^{13}C$ experienced a large (~1‰) decline in MIS 12, before a sharp rise into MIS 11 (Fig. 10B). The mean global $\delta^{13}C$ change from MIS 12 to 11 was twice the $\delta^{13}C$ change from the last glacial to Holocene; the contrast has been attributed to changes in water properties [102]. Accordingly, the MIS 12–11 transition is not only sharply defined by carbon isotopes but also by the largest global oxygen isotope shift in the last 6 Myr [103], represented by an ~2.5‰ $\delta^{18}O$ decrease at Site 1143 in the southern SCS (Fig. 10A).

As mentioned above, the MBE centered on MIS 11 ~0.4 Ma marks the onset of the late Quaternary regime of glacial cycles with enhanced glacial/interglacial contrast. Unlike the 1.6 Ma event or the MPT, however, profound reorganization of deep water related to the MBE has not been discovered. In general, global glacial SST progressively warmed from 0.9 Ma toward 0.5 Ma, before ending with a significant cooling at the MIS13/12 transition (Fig. 9). However, no major global thermal event

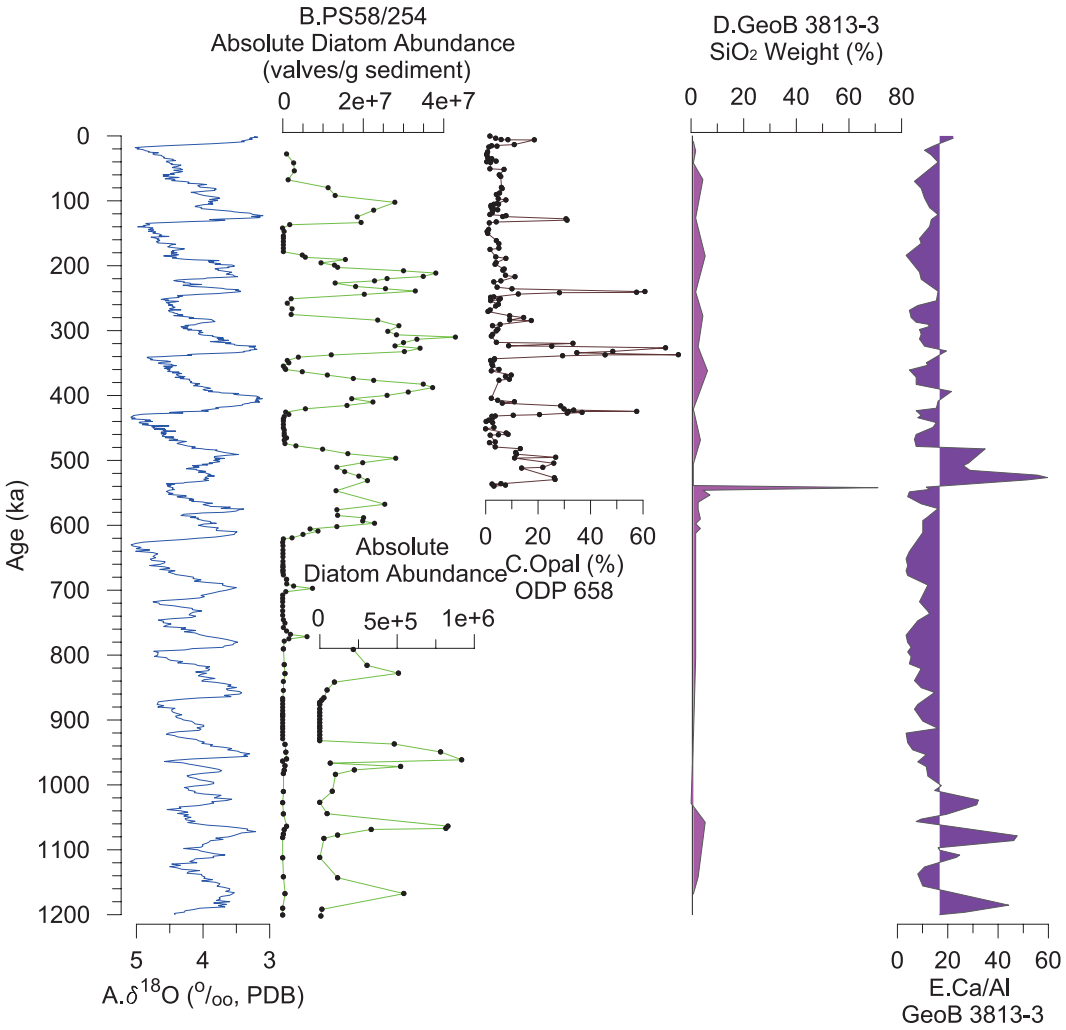

Figure 11. Diatom blooms in the last 1.2 Myr. (A) Benthic $\delta^{18}O$ stack of Lisiecki and Raymo [69]; (B) diatom abundance in core PS58/254, Southern Ocean (valves per gram of sediment), inset at the bottom highlights the variations in samples with low diatom content [82]; (C) opal% of carbonate-free silt, ODP Site 658, subtropical North Atlantic [99]; (D) biogenic silica (SiO2%) in core GeoB 3813–3, south Atlantic; (E) Ca/Al ratios in the same core [100].

occurred with the MBE itself around 0.4 Ma [94]. Moreover, interglacial environmental perturbations before and after the MBE (MIS 11) were more substantial than glacials [104,96], as post-MBE interglacials were much warmer than pre-MBE 'lukewarm' stages.

Regarding biological and biogeochemical aspects, the mid-Brunhes transition was a much longer process, beginning at MIS 13 during the $\delta^{13}C_{max\text{-}II}$. From MIS 13 to MIS 8, the global ocean saw coccolithophore blooms and carbonate dissolution, hence the term 'mid-Brunhes dissolution interval' [80]. This was a period when the coccolithophore assemblages, dominated by small-sized *Gephyrocapsa*, reached very high abundance in the global ocean. In the SCS, for example, the small-sized *Gephyrocapsa* species made up 1/3 to 2/5 of the nannofossil flora from MIS 13 to MIS 8 (Fig. 12B) [87], correlating well with the maximum values of coccolith $\delta^{13}C$, which is also a proxy of productivity (Fig. 12G and H) [105]. This stage of *Gephyrocapsa* proliferation has been proven global in nature, but its beginning is somehow diachronous, since it probably occurred earlier in the high-latitude North Atlantic (Fig. 12) [106,83]. The interval of the coccolithophore bloom coincides with global carbonate dissolution, which is distinctly manifested by coarse fraction curves from various sites (Fig. 13A–E) [13,109,110] and shell weight changes of planktonic foraminifer *Globigerina bulloides* from the North Atlantic, indicating intensive biogeochemical activities (Fig. 13K) [80].

Hypothetical interactions between physical and biogeochemical processes

The foregoing discussions demonstrate two similar sequences of events leading to major transitions in Quaternary environmental evolution. The

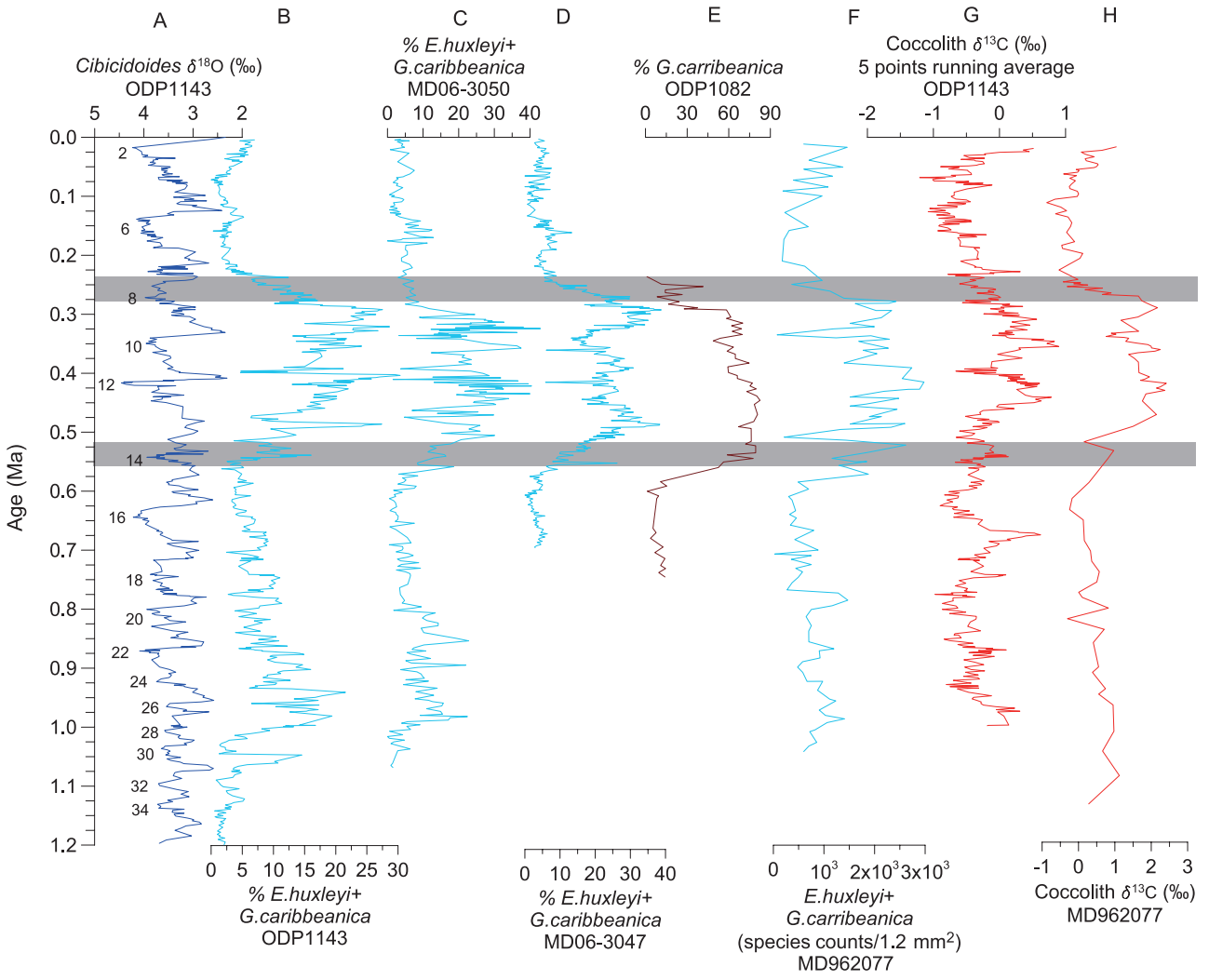

Figure 12. Proliferation of small-sized coccolithophore *Gephyrocapsa* in the late Pleistocene. (A) Benthic δ^{13}C at ODP Site 1143, SCS [3]; (B) *E. huxleyi* + *G. caribbeanica* (%) at ODP Site 1143, SCS [87]; (C) *E. huxleyi* + *G. caribbeanica* (%) at MD06–3050, Western Philippine Sea [107]; (D) *E. huxleyi* + *G. caribbeanica* (%) at MD06–3047, Western Philippine Sea [107]; (E) *G. caribbeanica* (%) at ODP Site 1082, South Atlantic [108]; (F) *E. huxleyi* + *G. caribbeanica* (Species counts 1.2 mm^{-2}) at MD962072, Indian Ocean [83]; (G) Coccolith δ^{13}C (five points running average), ODP Site 1143, SCS [87]; (H) Coccolith δ^{13}C at MD962072, Indian Ocean [83].

first lasted from MIS 31 to MIS 21 (1.08–0.82 Ma) including $\delta^{13}C_{max\text{-}III}$ and MPT, and the second from MIS 15 to MIS 11 (0.62–0.40 Ma) including $\delta^{13}C_{max\text{-}II}$ and MBE (Table 2). Both started with an unusual warm and long interglacial, namely, the 30-kyr long interglacial of MIS 31 when the West Antarctic ice sheet collapsed [84], and the 'super-interglacial' MIS 15–13 with a possible collapse of that ice sheet [97]. These abnormal warming intervals were subsequently followed by the corresponding $\delta^{13}C_{max\text{-}III}$ event in MIS 29–25 (0.96–1.04 Ma) and $\delta^{13}C_{max\text{-}II}$ event at MIS 13 (0.53–0.47 Ma), respectively. After a stage of steep decline in both δ^{13}C and δ^{18}O, the critical point of regime shift in glacial cyclicity occurred: the MPT (~0.9 Ma) and MBE (~0.4 Ma), each beginning with an extremely enlarged volume of global ice sheets, followed by a rapid rebound to an unusual warm interglacial period (MIS 22/21 and MIS 12/11) (Table 2).

The parallel changes between the two groups of events are not mere coincidence, but imply a similar mechanism behind the sequence of events. Of particular importance is the potential connection between physical processes of ice-sheet volume changes and the biological processes represented by carbon isotope variations (see below). The parallelism, however, is by no means suggestive of an identical origin of the MPT and MBE, because the two groups of events varied in background and consequences. For example, the MPT was at the end of a long-term cooling and shifted the dominant periodicity of climate cycles, whereas the MBE was at the end of a long-term warming and only changed the variation amplitude of the cycles (Fig. 10). Many

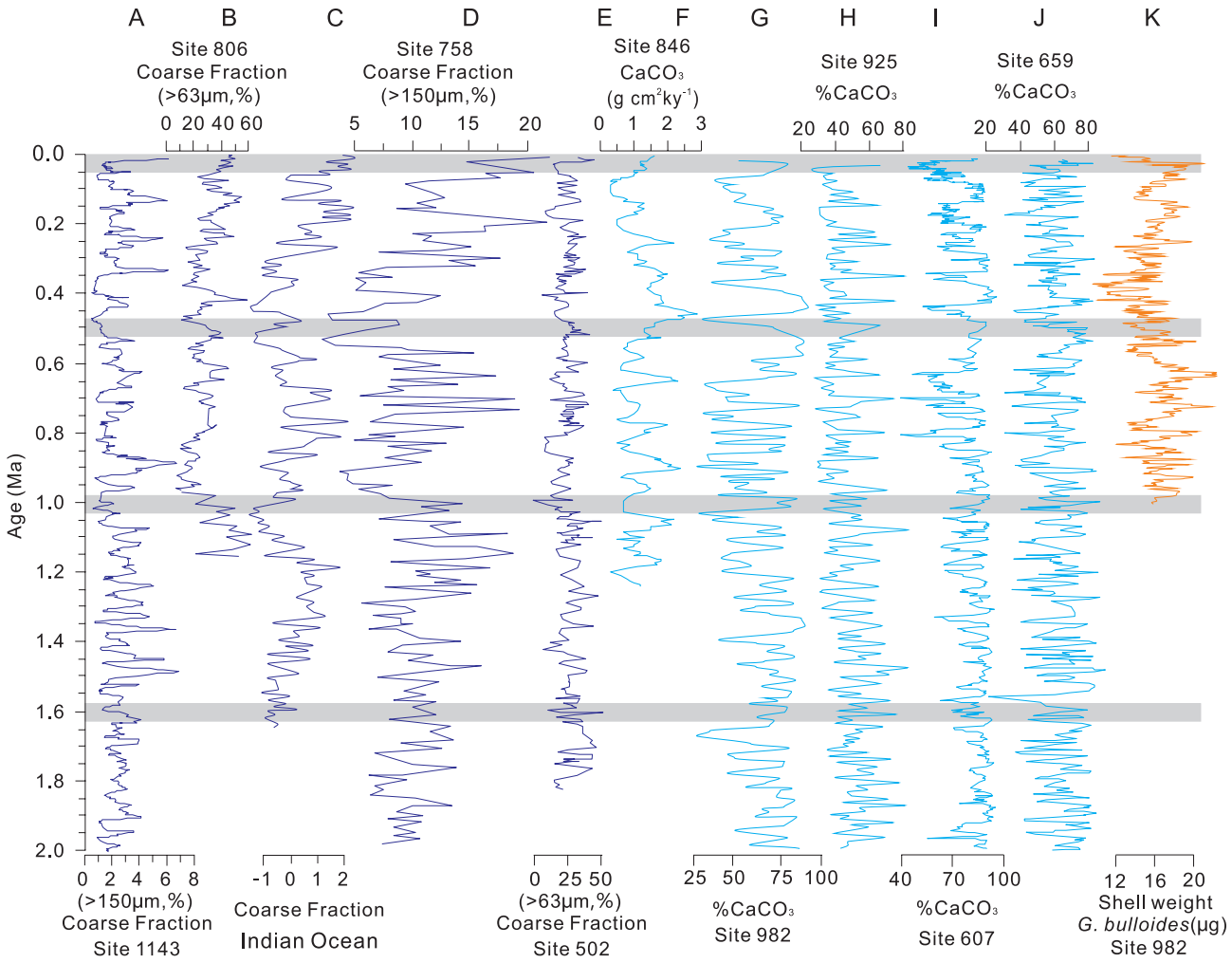

Figure 13. Carbonate deposition and preservation in the last 2 million years. (A–E) Coarse fraction (%): (A) ODP Site 1143, SCS, (>150 mm;) [4]; (B) ODP Site 806,West Pacific (>63 mm) [109]; (C) composite coarse fraction index, tropical Indian Ocean [13]; (D) ODP Site 758, Indian Ocean (>150 mm) [13]; (E) DSDP Site 502, Caribbean (>63 mm) [110]. F-J, $CaCO_3$%: (F) ODP Site 846, East Pacific (accumulation rate, mg cm^{-2} kyr^{-1}) [111]; (G) ODP Site 982, North Atlantic [112]; (H) ODP Site 925, North Atlantic [113]; (I) ODP Site 607 [114,115]; (J) ODP Site 659, North Atlantic [62]. (K) Shell weights of *Globigenina bulloides* from ODP Site 982, North Atlantic [80].

Table 2. Two groups of events in the Quaternary arranged in sequences of relevant MIS.

Events	MPT	MBE	SST
West Antarctic ice-sheet melting	31	15–13	Southern warming
Carbon isotope maximum	29–25	13	Relatively warm and stable
Global ice-sheet growth	22	12	Drastic cooling
Global ice-sheet melting	21	11	Drastic warming

authors believe a special environment existed between the MPT and MBE. This was either an 'MPT interim state' (0.5–1.0 Ma) [9], a period with 'sluggish deep western boundary currents' (0.45–0.85 Ma) [116] or a period of 'lukewarm interglacials' (0.45–0.8 Ma) [98].

Nevertheless, all the new findings boil down to the conclusion that the Quaternary environmental evolution is a continuing process. A climate event may not necessarily be caused by contemporary driving factors within a specific glacial cycle, but may be cultivated by previous changes from a long-term process. The MPT occurred at the end of a long-term glacial cooling shortly after 1.6 Ma, whereas the MBE was at the end of a glacial warming following the MPT (Figs 6 and 10). The abnormal environmental conditions in MIS 13, the prelude of MBE, are probably related to the new oceanographic pattern established at the end of the MPT [117]. The sequence of events also raises crucial questions regarding the relationship between $\delta^{13}C$ and $\delta^{18}O$. If the drastic changes in $\delta^{18}O$ were preceded by the $\delta^{13}C$max, did they have any causal tie? If the $\delta^{13}C$max followed major warming in the Southern Ocean, did ice melt trigger oceanic carbon reservoir changes? A variety of hypotheses have been proposed to interpret the observations, which attribute the long-term changes of Quaternary $\delta^{13}C$ to

variations in either phytoplankton [4], the Southern Ocean [5], ocean ventilation, or production and export ratio of organic and inorganic carbon [8]. Nevertheless, the origin of δ^{13}Cmax or long-term variations in δ^{13}C remains elusive. Because the origin of the long-term δ^{13}C cycles is the key to solving the above questions, we now investigate features and implications of those cycles.

EXPLORING THE MECHANISMS OF LONG-TERM CYCLES IN OCEANIC CARBON RESERVOIR

Long-eccentricity forcing in the pre-Quaternary ocean

Now we attempt to answer the question why did the long-eccentricity cycles disappeared in the Quaternary. We begin by explaining how the oceanic carbon reservoir responds to the orbital forcing of long-eccentricity in an ice-free world, or in relatively warm periods with insignificant ice-cap in the climate system.

(i) *Rain ratio hypothesis*. As has been known for nearly 30 yr, longer term δ^{13}C cycles reflect the effect of precession-cycle amplitude on climate and therefore on biomass [14]. The 400-kyr eccentricity cycles may indicate secular changes in 'rain ratio', which is the organic versus inorganic ratio of oceanic carbon deposition [118] dominated by the ratio of diatoms to coccoliths. Since diatoms produce only organic carbon, whereas coccolithophores generate both organic and inorganic carbon (calcite skeleton), a higher ratio of diatom/coccolith production would enhance the efficiency of the biological pump. Because the diatom/coccolith ratio depends on the availability of silica for biological uptake in the ocean and the major contribution of silica is from tropical rivers [119], long-term variations of oceanic δ^{13}C are ultimately related to low-latitude climate events such as monsoons [120]. The 'rain ratio' hypothesis appeared in line with the silica hypothesis of carbon balance in glacial cycles [121], as supported by most sediment evidence from the ocean, until the discovery of the role of ballast minerals (see below).

Because only late Pleistocene high-resolution marine isotope sequences were available, the longest cycle discerned ∼30 yr ago was the 100-kyr short eccentricity. But as André Berger noticed even earlier, astronomically, the most important eccentricity term has periodicity 413 kyr. He stated, 'if longer cores can be investigated by techniques allowing high resolution spectrum, I would expect … the main period of 413000a becoming strongly displayed' [122]. Indeed, his statement has been confirmed, and the 400-kyr cyclicity is better represented in the pre-Quaternary δ^{13}C records, likely because the eccentricity power is amplified in paleoclimate records (such as δ^{13}C) on an ice-free Earth much more than in the current Icehouse world [42]. Arguably, the ocean in the ice-free early Paleogene was much more homogeneous, so the oceanic carbon reservoir responded directly to orbital forcing, mainly to the precession modulated by the eccentricity [27,123]. As a result, the hydrological and biogeochemical cycles responding to eccentricity would do so in a coherent way. Because the residence time of carbon in the ocean– atmosphere–biosphere reservoir is $\sim 10^5$ yr, δ^{13}C changes in the global oceanic reservoir can only be clearly manifested on time scales exceeding this duration and are smoothed out at higher frequencies [27,28,124].

The rain ratio hypothesis in its original form, based on the functional types of phytoplankton or the diatom/coccolith ratio, is now challenged by the discovery of the 'ballast mineral' effect. It has been found that organic carbon sinking fluxes strongly correlate with mineral fluxes [125], and that most of the organic carbon rain in the deep sea is carried by calcium carbonate, because it is denser than opal and more abundant than terrigenous material [118]. This finding questions the role of function type in the biological pump by demonstrating that diatoms have no advantage over coccolithophores in transferring organic carbon to the deep-sea bottom. Invalidating the diatom-based hypothesis, the new finding also helps revise our understanding of POC flux to the ocean interior and of factors controlling the biological pump [126]. The rain ratio hypothesis, however, can still hold for oceanic δ^{13}C changes in general. Nevertheless, a new mechanism alternative to the diatom/coccolith ratio may be needed for interpreting long-term δ^{13}C changes.

(ii) *Microbial carbon pump and 'dissolved organic carbon hypothesis'*. Recent progress in microbial oceanography has revealed a remarkable yet unexplored role of the microbial carbon pump (MCP) in the oceanic carbon cycle. Marine DOC is the largest reservoir of reduced carbon in seawater and mostly persists over long periods ($\geq 10^3$ kyr) in the ocean as 'refractory DOC'. The MCP concept ascribes DOC production to microbial processes, and distinguishes two types of cycling of newly generated organic carbon in the ocean, namely

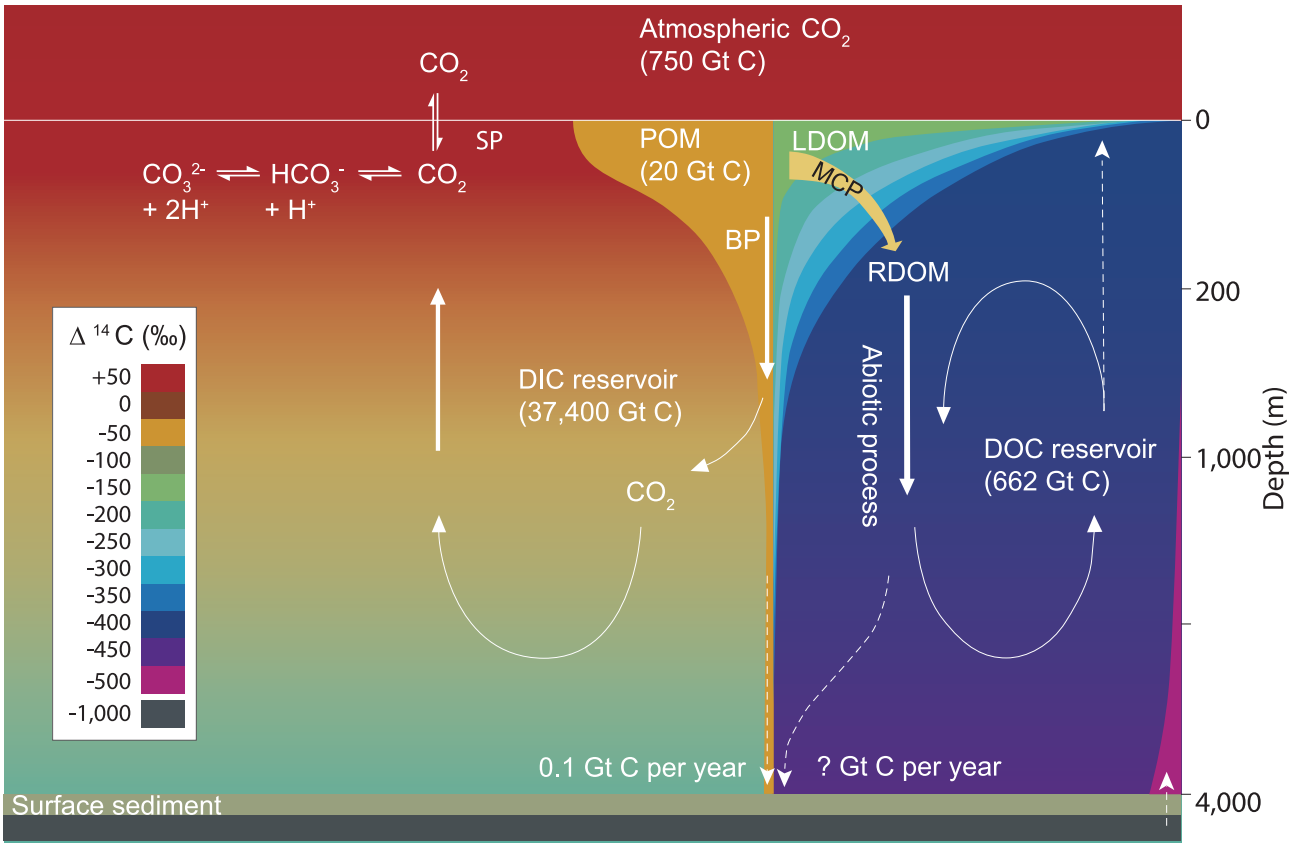

Figure 14. Formation of oceanic carbon reservoirs. DIC (left) comprises the biggest reservoir, while the DOC reservoir (right) formed by RCOM is comparable to the atmospheric CO_2 inventory by size. Background colors indicate radiocarbon $\Delta^{14}C$. Note that $\Delta^{14}C$ is related but not equal to age, with −1000 in $\Delta^{14}C$ corresponds to ∼50 000 in ^{14}C year [127].

rapid and slow cycles related to the biological pump and MCP, respectively. The rapid cycle is driven by photosynthesis and subsequent POC sedimentation through the biological pump, whereas the slow cycle is mediated by the MCP, prolonging the residence time of carbon in the ocean (Fig. 14) [127]. Since microbes generate refractory DOC that is resistant to biological decomposition and assimilation and can thereby persist in the water column, the MCP concept identifies a dissolved phase sequestration mechanism in the ocean, parallel to the burial of POC in bottom sediments [128].

As the largest pool of organic carbon in the ocean, oceanic DOC modulates $\delta^{13}C$ values of ocean water mainly through variations in its amount and hence the POC/DOC ratio. In the modern ocean, DOC ^{14}C age averages ∼5000 yr, but the lifetime of recalcitrant DOC is ∼16 000 yr according to modeling results, or even ∼40 000 yr for 'ultra-refractory DOC' [129]. Old carbon in the deep ocean is not necessarily produced by microbes in the water column, because there is DOC originating from the deep biosphere below the sea floor [130]. Nonetheless, DOC in the ocean may have been much more persistent in the geological past, when the ocean was dynamically more stable or stratified. Consequently, waxing and waning of the ocean DOC reservoir may have been significant in carbon cycling through geological history and left their imprints in $\delta^{13}C$ records, as amply supported by evidence.

The DOC reservoir in the deep-time ocean may have been much larger than in the modern one. For example, 'hyperthermal' events ∼50 Myr ago saw the mineralization of refractory DOC in the ocean with greater mass than the entire modern DOC reservoir over ∼30 000 yr [131]. Furthermore, the Proterozoic-ocean-dissolved organic matter inventory was presumably larger by orders of magnitude than that exists today [132]. This may explain why ocean water $\delta^{13}C$ had much larger amplitude fluctuations, reaching >10‰ in the Neoproterozoic and >1‰ in the early Cenozoic, compared with only ∼0.3–0.5‰ in the Plio-Pleistocene (see below).

Since DOC is biogenic in the euphotic upper ocean and can be removed by microbial mineralization in the deep ocean, DOC concentrations therefore decrease downward in the ocean and can be

transported great distances, eventually being redistributed in deep current systems. As a result, the DOC distribution in the ocean closely follows water circulation [133]. Biogeographically, photosynthetic microbes prevail in oligotrophic subtropical waters [134], which also have the highest DOC concentration [135]. This is in agreement with time-series observations showing that the oligotrophic open ocean is heterotrophic and dominated by small phytoplankton of microbes. However, this background state can be interrupted by a 'nutrient-excited state', when the rapid introduction of new nutrients into the system leads to the development of large eukaryote phytoplankton populations and episodic autotrophy [136,137]. This is exactly what happens in the Atlantic and Pacific subtropical gyres; for instance, prior to the δ^{13}Cmax events when laminated diatom ooze layers accumulated (see 'Carbon isotope maximum-II and mid-brunhes event' section).

In sum, the POC/DOC ratio of the ocean is heavily nutrient dependent. An enhanced input of nutrients may foster a nutrient-excited state in the otherwise oligotrophic ocean, increase the POC/DOC ratio and subsequently lighten δ^{13}C values in ocean water. As in the above discussion, the long-eccentricity cycles in the oceanic carbon reservoir may have a monsoonal origin, and likely played a part in creating such nutrient-excited states.

Therefore, we propose a DOC hypothesis, with the basic concept briefly summarized as follows (also shown in Fig. 15). We leave detailed argumentation of the hypothesis to be published elsewhere. At the long-eccentricity maximum, summer insolation maximizes at low latitudes and regional and global seasonality increase. This results in an intensified global monsoon and enhanced precipitation, which boosts both chemical weathering on land and river runoff, increasing nutrient input to the ocean. In the nutrient-excited ocean, eukaryote large phytoplankton is stimulated and surface productivity increases, which in turn raises the POC/DOC ratio and diminishes δ^{13}C in ocean water (Fig. 15).

The hypothetical connection between eccentricity forcing and long-term changes of δ^{13}C can be demonstrated through numerical simulation, using a seven-box model for the Miocene climate optimum of 14–17 Ma with only a minor ice-sheet influence. The simulation results show that eccentricity maxima (minima) enhance (reduce) weathering intensity and nutrient supply, which lead to the minima (maxima) of δ^{13}C in the ocean (Fig. 4D) [24].

However, the sensitivity of oceanic δ^{13}C to orbital forcing at the 400-kyr frequency varies with time [42], and the long-eccentricity cycles in the global δ^{13}C records are obscured after 1.6 Ma and replaced by longer cycles [7]. Since the main theme herein is the Quaternary ocean, we focus on the advantage of the DOC hypothesis for the recent past, especially its ability to interpret both the regular δ^{13}C cycle at 400 kyr and prolonged 500-kyr cycle in the Pleistocene.

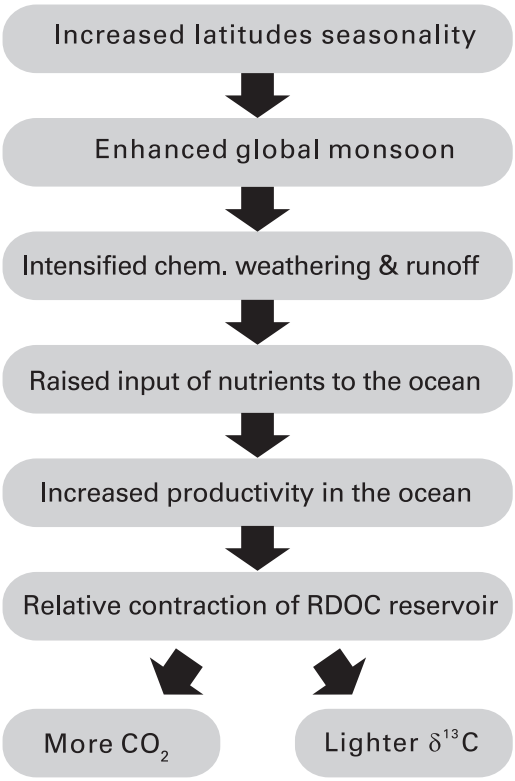

Figure 15. The DOC hypothesis for the long-eccentricity cycle of oceanic δ^{13}C.

Hypothetical origin of long-term δ^{13}C cycles in the Quaternary

(i) *Role of the Southern Ocean*. As described in the 'From the 2.7 Ma event to 1.6 Ma event' section, the conspicuous features of the 1.6 Ma event are the hydrologic separation of the abyss from the upper Southern Ocean (Fig. 7) and the obscuration of 400-kyr long-eccentricity cycles in δ^{13}C (Fig. 3). These two events may be related, in that the development of large bipolar ice sheets changed the hydrology of the Southern Ocean, and subsequent oceanic response to long-eccentricity forcing was different for an ice-capped Earth than for the earlier ice-free Earth [7].

Since the modern Southern Ocean is the most important region for controlling atmospheric CO_2 by serving as a lid to the larger volume of the deep ocean [48], the ultimate formation of the chemical divide 1.6 Myr ago may have greatly enhanced the role of this ocean in

global carbon cycling. There are many ways for the Southern Ocean to affect the oceanic carbon reservoir [138]. For example, a retreat of ice coverage may increase the open-water area and raise productivity, but nutrient redistribution is a crucial control on the efficiency of the biological pump of the global ocean and $\delta^{13}C$ of ocean water via the POC/DOC ratio. In the modern world, the Southern Ocean imposes the highest concentration of unused, so-called preformed nutrient on the interior and is thus responsible for most of the inefficiency of the global biological pump [138.] The 'leakage' of nutrient-rich waters from the Southern Ocean into lower latitudes stimulates bioproductivity and increases the POC/DOC ratio. Opal peaks have been reported near the western Antarctic Southern Ocean, from near the Antarctic Polar Front to the subtropical oceans during interglacial and glacial terminations (Fig. 11B and C) [82,99,139], but most striking is the discovery of diatom-mat deposits in low-latitude oligotrophic oceans.

Unlike normal diatom-rich deposits, the deposits there are laminated near-monospecific layers consisting of mat-forming and large-celled diatoms. These are so-called shade species adapted to stratified waters, capable of using deep nutrients, growing under low-light conditions and vertically migrating in the water column [140]. A valuable feature of the diatom of 'shade flora' is their occurrence in the oligotrophic oceans, such as in subtropical gyres. When entering the subsurface of the low-latitude ocean, the silica- and nutrient-rich water of the Southern Ocean may trigger a rapid burst of diatom-mat production and the deposition of laminated diatom layers, as recorded in the low-latitude Pacific and Atlantic.

Diatoms are a major component of the phytoplankton community, accounting for 40% of total primary production in the ocean and always dominating ocean biogeochemical cycles [141]. The role of mat-forming diatoms in carbon cycling in the modern and ancient ocean is seriously underestimated, owing to difficulties of observation and their sporadic distribution in the deep ocean. However, these diatoms may have been much more important in the geological past in a stratified deep ocean [140]. The biogeochemistry of diatom mats represents an overlooked process in oceanic carbon cycling, since it can turn oligotrophic water into the nutrient-excited state [136] and change the POC/DOC ratio in the ocean.

However, how does Southern Ocean water affect the oceanic carbon reservoir and $\delta^{13}C$ value of the global ocean on 10^5-yr time scale remains a largely unexplored process. The original version of the 'silica leakage' hypothesis, which ascribes glacial reduction of atmospheric CO_2 directly to silica leakage from the Southern Ocean [142], is now challenged by evaluative studies [143,144]. Nevertheless, the impact of this leakage on the ocean carbon reservoir is not negated, so the deposition of diatom mats may serve as one of the mechanisms causing the variations of oceanic $\delta^{13}C$.

What is the role of the microbial pump and DOC as newly found attributors to long-term $\delta^{13}C$ changes in interaction with diatom blooms? It remains unclear how the short-term production of diatom mats contributes to long-term changes in oceanic $\delta^{13}C$. Since any new production of POC by eukaryotic phytoplankton inevitably increases the amount of DOC, that DOC may have a surface distribution pattern opposite to that of the deep ocean [135]. Therefore, any straightforward response of the POC/DOC ratio to diatom-mat events may be difficult to interpret. At present, we can say that since the DOC distribution in the ocean is controlled by the circulation, the POC/DOC ratio in the global ocean is likely affected by hydrologic changes in the Southern Ocean more than in other ocean basins. Consequently, any large-scale retreat of the ice cap and leakage of nutrient-rich water may have changed the POC/DOC ratio and ultimately the oceanic $\delta^{13}C$.

(ii) *A new hypothesis for the Quaternary ocean*. In the foregoing, we demonstrated the possible connection of long-term cyclic changes of $\delta^{13}C$ with ice-sheet events in the Quaternary and proposed a DOC hypothesis to account for the long-term cycles. Such a hypothesis enables us to line up discrete events and pinpoint key issues in understanding the chain of changes in the Quaternary environment.

At the Plio-Pleistocene boundary, global cooling and the growth of ice sheets were coupled with a restructuring of the global ocean. The vertical stratification of the polar oceans at 2.7 Ma and its subsequent development not only isolated the abyss of the Southern Ocean to become the largest carbon reservoir of the global ocean, but also led to the zonal asymmetry of the equatorial Pacific at 1.6 Ma. Concomitantly, the reorganization of the ocean structure caused a southward 'opal shift' with high-rate diatom accumulation moving abruptly from the subarctic Pacific to the Southern Ocean. This occurred in an

interval called the 'late Pliocene–early Pleistocene productivity maximum' from 2.7 to 1.6 Ma, until a sharp productivity reduction in the low-latitude Pacific. The two-phase restructuring of the global ocean helped establish a glacial regime in the climate system. Before 1.6 Ma, both the climate record and oceanic δ^{13}C followed the 400-kyr long-eccentricity in response to orbital forcing. After that time, however, this 400-kyr rhythm became obscured (Fig. 3), when the orbital forcing of the oceanic carbon reservoir was suppressed by ice-sheet-related oceanographic processes. Regardless of the obscured δ^{13}C signal, the normal 400-kyr cycles persist in many other proxy records, such as the K/Al ratio representing the intensity of chemical weathering [22].

The obscuration of the long-eccentricity signal in isotopic records was not restricted to the Pleistocene, since the 400-kyr cycles of δ^{13}C were interrupted earlier in the Cenozoic. An example is the Middle Miocene cooling event, associated with the expansion of the Antarctic ice sheet. This event occurred abruptly at 13.9 Ma, immediately after the deposition of the middle Miocene Monterey formation with abundant inorganic carbon, and was accompanied by a sudden disappearance of 400-kyr cycles in δ^{13}C records (Fig. 4B) [23,25]. This implies a constant effect of the eccentricity cycle on the oceanic carbon reservoir, although its effectiveness is not always prominent in deep ocean δ^{13}C records, especially when the climate was locked in a major glacial mode such as in the Pleistocene.

Climate evolution through the Pleistocene included not only the growth of the ice sheets but also an enhanced role of the Southern Ocean in oceanic carbon cycling, which in turn enhanced the amplitude of δ^{18}O and δ^{13}C variations over glacial cycles. The $\delta^{13}C_{max\text{-}IV}$ around 1.6 Ma was followed by a long cooling trend in the global ocean, from ∼1.5 to 1.1 Ma (Fig. 9) until the 'super-interglacial' MIS 31, when the collapse of the West Antarctic ice sheet triggered a phytoplankton bloom. It remains unclear, however, how the warming episode in the south induced the chain of events leading to the MPT, as listed in Table 2. In the SCS, the MIS 31 warming was associated with spikes in SST and in *Gephyrocapsa* %. The subsequent warm and productive interval of $\delta^{13}C_{max\text{-}III}$ (MIS 29 to MIS 25) was followed by a negative shift of ∼1‰ of benthic δ^{13}C approaching MIS 23. This was before a major decline in δ^{18}O, heralding a major ice-sheet expansion at the MIS 23/22 transition, the core of the MPT (Fig. 10; Table 2).

The next group of events features $\delta^{13}C_{max\text{-}II}$ and MBE, starting immediately after the MPT. Again these began with a prolonged interglacial from MIS 15 to MIS 13, when the West Antarctic ice sheet likely collapsed. Diatom productivity in the Southern Ocean increased remarkably during several interglacials beginning in MIS 15, but the wide distribution of laminated diatom-mat deposits of MIS 14 under the Atlantic subtropical gyre deserves special attention (Fig. 11). As shown by the sediment sequence, diatom blooms in MIS 14 were succeeded by coccolithophore blooms (Fig. 11D and E), all indicative of high productivity in the oligotrophic ocean driven by the leakage of high-nutrient water from the Southern Ocean. The abnormal climatic and oceanographic conditions during MIS 13 or the $\delta^{13}C_{max\text{-}II}$ event have attracted the attention of many authors [117,145–147] who primarily attributed the origin of these hydroclimate changes to the Southern Ocean.

The event of MIS 13 or $\delta^{13}C_{max\text{-}II}$ preceded, and may have contributed to, a triple transition in the ice sheet, ocean alkalinity and phytoplankton evolution. That is, the ice sheet drastically enlarged and then shrank over MIS 12 and MIS 11, deep-sea carbonate underwent maximum dissolution in MIS 11, and there was a period of increased productivity in the global ocean marked by the proliferation of *Gephyrocapsa* from MIS 13 to MIS 8 (Fig. 10C). Although all events discussed above are potentially interrelated, further research is required to test these hypotheses and determine their potential linking mechanisms.

Special attention is warranted for the current carbon isotope maximum, $\delta^{13}C_{max\text{-}I}$. As seen in the compilation of δ^{13}C curves (Fig. 3), the Earth is currently passing through the current δ^{13}Cmax. If the two δ^{13}Cmax in the last million years presaged the significant development of glacial climate, what does the current δ^{13}Cmax mean for the long-term climate change in the future? Perhaps a fundamental difference is the fact that the current δ^{13}Cmax coincides with a long-eccentricity minimum, whereas the two previous δ^{13}Cmax events were out of phase with the long-eccentricity rhythms (Fig. 2). In any case, it is crucial to understand the nature of δ^{13}Cmax events and their impacts on the global climate and ocean. The biogeochemical aspects of δ^{13}C, culminating with δ^{13}Cmax events, await more concentrated scientific endeavors.

CONCLUSIONS

We have reviewed long-term processes influencing the oceanic carbon reservoir across glacial cycles, since these processes are closely related to long-eccentricity in orbital forcing and are best represented by δ^{13}C sequences largely driven by POC/DOC ratio variations in the ocean. Tracing the history of major environmental events in the

Quaternary, we showed that these comprise a continuing chain of events that are a largely ignored aspect in Quaternary studies. Further attention is called to the following issues:

(i) *Role of long-term processes.* Quaternary paleoclimatology initiated by the discovery of past glacials and glacial cycles at 10^4-yr time scale have been the focus of research over the last century. In recent years with the emergence of continuous high-resolution records from the longer geological past, increasing evidence underscores the significance of long-duration processes at the time scale of 10^5 yr or more. The interglacials are different not only because of their specific orbital parameters at a particular time, but also in the resulting long-duration processes that persist across several glacial cycles.

(ii) *Role of long-eccentricity.* The long-eccentricity of ∼400 kyr is the most outstanding rhythm in the geological history and is likened to the 'heartbeat' of the ocean system [28]. Because carbon has a residence time of 10^5 yr in the ocean, the long-eccentricity is best represented by oceanic δ^{13}C. The 400-kyr signal in the δ^{13}C sequences was obscured beginning in 1.6 Ma. At that time, the global ocean entered a glacial regime, with the Southern Ocean largely controlling the oceanic carbon reservoir and oceanic processes suppressing the eccentricity signal. Nevertheless, the oceanic carbon reservoir continued to show cyclic changes at the time scale of 10^5 yr, recognized as 500-kyr cycles between δ^{13}Cmax events over the last million years.

(iii) *Role of the Southern Ocean in long-term environmental changes.* It is unlikely a coincidence that the obscuration of the long-eccentricity signal in the δ^{13}C records at 1.6 Ma occurred with the formation of the 'chemical lid' of the Southern Ocean, and that both the MPT and MBE were prefaced by unusually warm interglacials in the Antarctic region. One of the crucial mechanisms may be the nutrient transfer from the Southern Ocean northward, which led to major changes in the biological pump of the global ocean.

(iv) *Role of DOC in the biological pump.* The long-eccentricity 400-kyr cycles of δ^{13}C hypothetically originate from POC/DOC ratio variations in the ocean, which in turn depend on global monsoon intensity. Since 1.6 Ma, the 400-kyr cyclicity of δ^{13}C has extended to ∼500 kyr, but the long-term changes should remain associated with the POC/DOC ratio variations. This assumption is supported by discoveries such as the occurrence of laminated diatom-mat deposits in the oligotrophic ocean and the opal maximum in the Southern Ocean. Nonetheless, it remains a topic of future study as to how the phytoplankton events contribute to the long-term cyclic changes of δ^{13}C.

ACKNOWLEDGEMENTS

We thank NianZhi Jiao for valuable discussions in preparing the manuscript, HanJie Sun for providing data, and JingJing Liu and JianHong Zhou for technical assistance. We also thank anonymous reviewers for their constructive comments that significantly improved the manuscript. This work was supported by the National Natural Science Foundation of China (91128000).

REFERENCES

1. Wang, P. Response of western Pacific marginal seas to glacial cycles: Paleoceanographic and sedimentological features. *Mar Geol* 1999; **156**: 5–39.
2. Wang, P, Prell, W and Blum, P *et al. Proceedings of the Ocean Drilling Program: Initial Reports*, Vol. 184. College Station, TX: Ocean Drilling Program, 2000.
3. Wang, P, Tian, J and Cheng, X *et al.* Carbon reservoir changes preceded major ice-sheet expansion at the mid-Brunhes event. *Geology* 2003; **31**: 239–42.
4. Wang, P, Tian, J and Cheng, X *et al.* Major Pleistocene stages in a carbon perspective: the South China Sea record and its global comparison. *Paleoceanography* 2004; **19**: PA4005.
5. Köhler, P and Bintanja, R. The carbon cycle during the Mid Pleistocene transition: the Southern Ocean Decoupling Hypothesis. *Clim Past* 2008; **4**: 311–32.
6. Russon, T, Paillard, D and Elliot, M. Potential origins of 400–500 kyr periodicities in the ocean carbon cycle: a box model approach. *Global Biogeochem Cy* 2010; **24**: GB2013.
7. Wang, P, Tian, J and Lourens, LJ. Obscuring of long eccentricity cyclicity in Pleistocene oceanic carbon isotope records. *Earth Planet Sci Lett* 2010; **290**: 319–30.
8. Hoogakker, B, Rohling, E and Palmer, M *et al.* Underlying causes for long-term global ocean δ^{13}C fluctuations over the last 1.20 Myr. *Earth Planet Sci Lett* 2006; **248**: 15–29.
9. Schmieder, F, von Dobeneck, T and Bleil, U. The mid-Pleistocene climate transition as documented in the deep South Atlantic Ocean: initiation, interim state and terminal event. *Earth Planet Sci Lett* 2000; **179**: 539–49.
10. Arrhenius, G. Properties of the sediment and their distribution. In: Pettersson, H, Jerlov, N and Kullenberg, B *et al.* (eds). *Reports of the Swedish Deep-Sea Expedition, 1947–1948: Sediment cores from the East Pacific*, Vol. 5. Gothenburg: Elanders Boktr, 1952, 1–89.
11. Briskin, M and Berggren, WA. Pleistocene stratigraphy and quantitative paleoceanography of tropical North Atlantic core V16–205. In: Saito, T and Burckle, L (eds). *Late Neogene Epoch boundaries.* New York: Micropaleontol Press, 1975; 167–98.

12. Droxler, A, Haddad, G and Mucciarone, D *et al.* Pliocene-Pleistocene aragonite cyclic variations in Holes 714A and 716B (the Maldives) compared with Hole 633A (the Bahamas): records of climate-induced $CaCO_3$ preservation at intermediate water depths. In: Duncan, RA, Backman, J and Peterson, LC *et al.* (eds). *Proceedings of the Ocean Drilling Program, Scintific Results*, Vol. 115. College Station, TX: Ocean Drilling Program, 1990, 539–77.
13. Bassinot, FC, Beaufort, L and Vincent, E *et al.* Coarse fraction fluctuations in pelagic carbonate sediments from the tropical Indian Ocean: a 1500-kyr record of carbonate dissolution. *Paleoceanography* 1994; **9**: 579–600.
14. Keigwin, LD and Boyle, EA. Carbon isotopes in deep-sea benthic foraminifera: precession and changes in low-latitude biomass. *Geoph Monog Series* 1985; **32**: 319–28.
15. Raymo, M, Ruddiman, W and Shackleton, N *et al.* Evolution of Atlantic-Pacific $\delta^{13}C$ gradients over the last 2.5 m.y. *Earth Planet Sci Lett* 1990; **97**: 353–68.
16. Bickert, T, Berger, W and Burke, S *et al.* Late Quaternary stable isotope record of benthic foraminifers: Sites 805 and 806, Ontong Java Plateau 1. In: Berger, WH., Kroenke, LW and Mayer, LA *et al.* (eds). *Proceedings of the Ocean Drilling Program, Science Results*, Vol. 130. College Station, TX: Ocean Drilling Program, 1993, 411–20.
17. Mix, AC, Pisias, NG and Rugh, W Benthic foraminifer stable isotope record from site 849 (0–5 Ma): local and global climate changes. In: Pisias, NG, Mayer, LA and Janecek, TR *et al.* (eds). *Proceedings of the Ocean Drilling Program, Science Results*, Vol. 138. College Station, TX: Ocean Drilling Program, 1995, 371–412.
18. Kukla, G and Cílek, V. Plio-pleistocene megacycles: record of climate and tectonics. *Palaeogeogr Palaeocl* 1996; **120**: 171–94.
19. Xiong, S, Jiang, W and Liu, T. Mega-pulses and megacycles in East Asian monsoon variations recorded in Chinese loess-red clay magnetic susceptibility. *Geophys Res Lett* 2006; **33**: L18702.
20. Tian, J, Zhao, Q and Wang, P *et al.* Astronomically modulated Neogene sediment records from the South China Sea. *Paleoceanography* 2008; **23**: PA3210.
21. Wehausen, R and Brumsack, H-J. Astronomical forcing of the East Asian monsoon mirrored by the composition of Pliocene South China Sea sediments. *Earth Planet Sci Lett* 2002; **201**: 621–36.
22. Tian, J, Xie, X and Ma, W *et al.* X-ray fluorescence core scanning records of chemical weathering and monsoon evolution over the past 5 Myr in the southern South China Sea. *Paleoceanography* 2011; **26**: PA4202.
23. Holbourn, A, Kuhnt, W and Schulz, M *et al.* Orbitally-paced climate evolution during the middle Miocene 'Monterey' carbon-isotope excursion. *Earth Planet Sci Lett* 2007; **261**: 534–50.
24. Ma, W, Tian, J and Li, Q *et al.* Simulation of long eccentricity (400-kyr) cycle in ocean carbon reservoir during Miocene Climate Optimum: weathering and nutrient response to orbital change. *Geophys Res Lett* 2011; **38**: L10701.
25. Tian, J, Shevenell, A and Wang, P *et al.* Reorganization of Pacific Deep Waters linked to middle Miocene Antarctic cryosphere expansion: a perspective from the South China Sea. *Palaeogeogr Palaeocl* 2009; **284**: 375–82.
26. Matthews, R and Frohlich, C. Maximum flooding surface and sequence boundaries: comparisons between observation and orbital forcing in the Cretaceous and Jurassic (65–190 Ma). *Geoarabia* 2002; **7**: 503–38.
27. Cramer, BS, Wright, JD and Kent, DV *et al.* Orbital climate forcing of $\delta^{13}C$ excursions in the late Paleocene–early Eocene (chrons C24n–C25n). *Paleoceanography* 2003; **18**: 1097.
28. Pälike, H, Norris, RD and Herrle, JO *et al.* The heartbeat of the Oligocene climate system. *Science* 2006; **314**: 1894–8.
29. Fischer, G and Schwarzacher, W. Cretaceous bedding rhythms under orbital control? In: Berger, J, Imbrie, J and Hays, J *et al.* (eds). *Milankovitch and Climate*. Dordrecht: Reidel, 1984, 163–76.
30. Herbert, TD, Stallard, R and Fischer, AG. Anoxic events, productivity rhythms, and the orbital signature in a Mid-Cretaceous deep-sea sequence from central Italy. *Paleoceanography* 1986; **1**: 495–506.
31. Herbert, TD. Milankovitch climatic origin of mid-Cretaceous black shale rhythms in central Italy. *Nature* 1986; **321**: 739–43.
32. Moore, T, Pisias, N and Dunn, D. Carbonate time series of the Quaternary and Late Miocene sediments in the Pacific Ocean: a spectral comparison. *Mar Geol* 1982; **46**: 217–33.
33. Latta, DK, Anastasio, DJ and Hinnov, LA *et al.* Magnetic record of Milankovitch rhythms in lithologically noncyclic marine carbonates. *Geology* 2006; **34**: 29–32.
34. Giorgioni, M, Weissert, H and Bernasconi, SM *et al.* Orbital control on carbon cycle and oceanography in the mid-Cretaceous greenhouse. *Paleoceanography* 2012; **27**: PA1204.
35. Husson, D, Galbrun, B and Laskar, J *et al.* Astronomical calibration of the Maastrichtian (Late Cretaceous). *Earth Planet Sci Lett* 2011; **305**: 328–40.
36. Batenburg, SJ, Sprovieri, M and Gale, AS *et al.* Cyclostratigraphy and astronomical tuning of the Late Maastrichtian at Zumaia (Basque country, Northern Spain). *Earth Planet Sci Lett* 2012; **359–360**: 264–78.
37. Pälike, H, Frazier, J and Zachos, JC. Extended orbitally forced palaeoclimatic records from the equatorial Atlantic Ceara Rise. *Quaternary Sci Rev* 2006; **25**: 3138–49.
38. Westerhold, T, Röhl, U and Raffi, I *et al.* Astronomical calibration of the Paleocene time. *Palaeogeogr Palaeocl* 2008; **257**: 377–403.
39. Westerhold, T, Röhl, U and Laskar, J. Time scale controversy: accurate orbital calibration of the early Paleogene. *Geochem Geophy Geosy* 2012; **13**: Q06015.
40. Dinarès-Turell, J, Baceta, JI and Pujalte, V *et al.* Untangling the Palaeocene climatic rhythm: an astronomically calibrated Early Palaeocene magnetostratigraphy and biostratigraphy at Zumaia (Basque basin, northern Spain). *Earth Planet Sci Lett* 2003; **216**: 483–500.
41. Paul, HA, Zachos, JC and Flower, BP *et al.* Orbitally induced climate and geochemical variability across the Oligocene/Miocene boundary. *Paleoceanography* 2000; **15**: 471–85.
42. Zachos, JC, Shackleton, NJ and Revenaugh, JS *et al.* Climate response to orbital forcing across the Oligocene-Miocene boundary. *Science* 2001; **292**: 274–8.
43. Coxall, HK, Wilson, PA and Pälike, H *et al.* Rapid stepwise onset of Antarctic glaciation and deeper calcite compensation in the Pacific Ocean. *Nature* 2005; **433**: 53–7.
44. Boulila, S, Galbrun, B and Miller, KG *et al.* On the origin of Cenozoic and Mesozoic 'third-order' eustatic sequences. *Earth-Sci Rev* 2011; **109**: 94–112.
45. Maslin, M, Li, X and Loutre, M-F *et al.* The contribution of orbital forcing to the progressive intensification of Northern Hemisphere glaciation. *Quaternary Sci Rev* 1998; **17**: 411–26.
46. Jansen, E, Fronval, T and Rack, F *et al.* Pliocene-Pleistocene ice rafting history and cyclicity in the Nordic Seas during the last 3.5 Myr. *Paleoceanography* 2000; **15**: 709–21.
47. Haug, GH, Ganopolski, A and Sigman, DM *et al.* North Pacific seasonality and the glaciation of North America 2.7 million years ago. *Nature* 2005; **433**: 821–5.
48. Marinov, I, Gnanadesikan, A and Toggweiler, J *et al.* The Southern Ocean biogeochemical divide. *Nature* 2006; **441**: 964–7.

49. Hodell, DA and Venz-Curtis, KA. Late Neogene history of deepwater ventilation in the Southern Ocean. *Geochem Geophy Geosy* 2006; **7**: Q09001.
50. Sigman, DM, Jaccard, SL and Haug, GH. Polar ocean stratification in a cold climate. *Nature* 2004; **428**: 59–63.
51. Herbert, TD, Peterson, LC and Lawrence, KT *et al.* Tropical ocean temperatures over the past 3.5 million years. *Science* 2010; **328**: 1530–4.
52. Li, L, Li, Q and Tian, J *et al.* A 4-Ma record of thermal evolution in the tropical western Pacific and its implications on climate change. *Earth Planet Sci Lett* 2011; **309**: 10–20.
53. Brierley, CM, Fedorov, AV and Liu, Z *et al.* Greatly expanded tropical warm pool and weakened Hadley circulation in the early Pliocene. *Science* 2009; **323**: 1714–8.
54. Sosdian, S and Rosenthal, Y. Deep-sea temperature and ice volume changes across the Pliocene-Pleistocene climate transitions. *Science* 2009; **325**: 306–10.
55. Wara, MW, Ravelo, AC and Delaney, ML. Permanent El Niño-like conditions during the Pliocene warm period. *Science* 2005; **309**: 758–61.
56. Li, LQ, Wang, Hui and Wang, Pinxian. Plio-Pleistocene productivity in southern South China Sea: implication for the ocean circulation variability, unpublished manuscript.
57. Lawrence, KT, Liu, Z and Herbert, TD. Evolution of the eastern tropical Pacific through Plio-Pleistocene glaciation. *Science* 2006; **312**: 79–83.
58. Etourneau, J, Martinez, P and Blanz, T *et al.* Pliocene–Pleistocene variability of upwelling activity, productivity, and nutrient cycling in the Benguela region. *Geology* 2009; **37**: 871–4.
59. Haug, GH, Sigman, DM and Tiedemann, R *et al.* Onset of permanent stratification in the subarctic Pacific Ocean. *Nature* 1999; **401**: 779–82.
60. Lange, C, Berger, W and Lin, H-L *et al.* The early Matuyama Diatom Maximum off SW Africa, Benguela Current System (ODP Leg 175). *Mar Geol* 1999; **161**: 93–114.
61. Demenocal, PB. African climate change and faunal evolution during the Pliocene–Pleistocene. *Earth Planet Sci Lett* 2004; **220**: 3–24.
62. Tiedemann, R, Sarnthein, M and Shackleton, NJ. Astronomic timescale for the Pliocene Atlantic $\delta^{18}O$ and dust flux records of Ocean Drilling Program Site 659. *Paleoceanography* 1994; **9**: 619–38.
63. Venz, KA and Hodell, DA. New evidence for changes in Plio–Pleistocene deep water circulation from Southern Ocean ODP Leg 177 Site 1090. *Palaeogeogr Palaeocl* 2002; **182**: 197–220.
64. Ravelo, AC, Andreasen, DH and Lyle, M *et al.* Regional climate shifts caused by gradual global cooling in the Pliocene epoch. *Nature* 2004; **429**: 263–7.
65. Fedorov, A, Dekens, P and McCarthy, M *et al.* The Pliocene paradox (mechanisms for a permanent El Niño). *Science* 2006; **312**: 1485–9.
66. Martínez-Garcia, A, Rosell-Melé, A and McClymont, EL *et al.* Subpolar link to the emergence of the modern Equatorial Pacific cold tongue. *Science* 2010; **328**: 1550–3.
67. Diekmann, B, Fälker, M and Kuhn, G. Environmental history of the southeastern South Atlantic since the Middle Miocene: evidence from the sedimentological records of ODP Sites 1088 and 1092. *Sedimentology* 2003; **50**: 511–29.
68. Cortese, G and Gersonde, R. Plio/Pleistocene changes in the main biogenic silica carrier in the Southern Ocean, Atlantic Sector. *Mar Geol* 2008; **252**: 100–10.
69. Lisiecki, LE and Raymo, ME. A Pliocene-Pleistocene stack of 57 globally distributed benthic $\delta^{18}O$ records. *Paleoceanography* 2005; **20**;PA1003.
70. Rutherford, S and D'Hondt, S. Early onset and tropical forcing of 100,000-year Pleistocene glacial cycles. *Nature* 2000; **408**: 72–5.
71. Clark, PU, Archer, D and Pollard, D *et al.* The middle Pleistocene transition: characteristics, mechanisms, and implications for long-term changes in atmospheric pCO_2. *Quaternary Sci Rev* 2006; **25**: 3150–84.
72. Zheng, F, Li, Q and Li, B *et al.* A millennial scale planktonic foraminifer record of the mid-Pleistocene climate transition from the northern South China Sea. *Palaeogeogr Palaeocl* 2005; **223**: 349–63.
73. Jin, H and Jian, Z. Millennial-scale climate variability during the mid-Pleistocene transition period in the northern South China Sea. *Quaternary Sci Rev* 2013; **70**: 15–27.
74. Li, Q, Wang, P and Zhao, Q *et al.* Paleoceanography of the mid-Pleistocene South China Sea. *Quaternary Sci Rev* 2008; **27**: 1217–33.
75. Hönisch, B, Hemming, NG and Archer, D *et al.* Atmospheric carbon dioxide concentration across the mid-Pleistocene transition. *Science* 2009; **324**: 1551–4.
76. Meyers, SR and Hinnov, LA. Northern Hemisphere glaciation and the evolution of Plio-Pleistocene climate noise. *Paleoceanography* 2010; **25**: PA3207.
77. Lawrence, KT, Sosdian, S, White, HE and Rosenthal, Y. North Atlantic climate evolution through the Plio-Pleistocene climate transitions. *Earth Planet Sci Lett* 2011; **300**: 329–42.
78. Elderfield, H, Ferretti, P and Greaves, M *et al.* Evolution of ocean temperature and ice volume through the mid-Pleistocene climate transition. *Science* 2012; **337**: 704–9.
79. McClymont, EL, Sosdian, SM and Rosell-Melé, A *et al.* Pleistocene sea-surface temperature evolution: early cooling, delayed glacial intensification, and implications for the mid-Pleistocene climate transition. *Earth-Sci Rev* 2013; **123**: 173–93.
80. Barker, S, Archer, D and Booth, L *et al.* Globally increased pelagic carbonate production during the Mid-Brunhes dissolution interval and the CO_2 paradox of MIS 11. *Quaternary Sci Rev* 2006; **25**: 3278–93.
81. Rackebrandt, N, Kuhnert, H and Groeneveld, J *et al.* Persisting maximum Agulhas leakage during MIS 14 indicated by massive Ethmodiscus oozes in the subtropical South Atlantic. *Paleoceanography* 2011; **26**: PA3202.
82. Konfirst, MA, Scherer, RP and Hillenbrand, CD *et al.* A marine diatom record from the Amundsen Sea—insights into oceanographic and climatic response to the Mid-Pleistocene transition in the West Antarctic sector of the Southern Ocean. *Mar Micropaleontol* 2012; **92**: 40–51.
83. Rickaby, R, Bard, E and Sonzogni, C *et al.* Coccolith chemistry reveals secular variations in the global ocean carbon cycle? *Earth Planet Sci Lett* 2007; **253**: 83–95.
84. Pollard, D and DeConto, RM. Modelling west antarctic ice sheet growth and collapse through the past five million years. *Nature* 2009; **458**: 329–32.
85. Scherer, R, Bohaty, S and Dunbar, R *et al.* Antarctic records of precession-paced insolation-driven warming during early Pleistocene Marine Isotope Stage 31. *Geophys Res Lett* 2008; **35**: L03505.
86. Grigorov, I, Pearce, RB and Kemp, AE. Southern Ocean laminated diatom ooze: mat deposits and potential for palaeo-flux studies, ODP leg 177, Site 1093. *Deep-Sea Res Pt II* 2002; **49**: 3391–407.
87. Liu, C, Yu, W, Tian, J and Wang, P. 5 Ma coccolith records and their paleoceanographical significance in the southern South China Sea, unpublished manuscript.
88. Tian, J, Wang, P and Cheng, X *et al.* Astronomically tuned Plio–Pleistocene benthic $\delta^{18}O$ record from South China Sea and Atlantic–Pacific comparison. *Earth Planet Sci Lett* 2002; **203**: 1015–29.
89. McClymont, EL and Rosell-Melé, A. Links between the onset of modern Walker circulation and the mid-Pleistocene climate transition. *Geology* 2005; **33**: 389–92.

90. Crowley, TJ. Late Quaternary carbonate changes in the North Atlantic and Atlantic/Pacific comparisons. In: Sundquist, ET and Broecker, WS (eds). *The Carbon Cycle and Atmospheric CO_2: Natural Variations Archean to Present. Geophysical Monograph Series*, Vol. 32. Washington: AGU, 1985, 271–84.
91. Jansen, J, Kuijpers, A and Troelstra, S. A mid-Brunhes climatic event: long-term changes in global atmosphere and ocean circulation. *Science* 1986; **232**: 619–22.
92. Droxler, AW, Bruce, CH and Sager, WW *et al.* Pliocene-Pleistocene variations in aragonite content and planktonic oxygen-isotope record in Bahamian periplatform ooze, Hole 633A. In: Austin, JA and Schlager, W *et al.* (eds). *Proceedings of the Ocean Drilling Program, Science Results*, Vol. 101. College Station, TX: Ocean Drilling Program, 1988, 221–44.
93. Lüthi, D, Le Floch, M and Bereiter, B *et al.* High-resolution carbon dioxide concentration record 650,000–800,000 years before present. *Nature* 2008; **453**: 379–82.
94. Candy, I, Coope, G and Lee, J *et al.* Pronounced warmth during early middle Pleistocene interglacials: investigating the mid-Brunhes event in the British terrestrial sequence. *Earth-Sci Rev* 2010; **103**: 183–96.
95. Hao, Q, Wang, L and Oldfield, F *et al.* Delayed build-up of Arctic ice sheets during 400,000-year minima in insolation variability. *Nature* 2012; **490**: 393–6.
96. Yin, Q. Insolation-induced mid-Brunhes transition in Southern Ocean ventilation and deep-ocean temperature. *Nature* 2013; **494**: 222–5.
97. Hillenbrand, C-D, Kuhn, G and Frederichs, T. Record of a mid-Pleistocene depositional anomaly in West Antarctic continental margin sediments: an indicator for ice-sheet collapse? *Quaternary Sci Rev* 2009; **28**: 1147–59.
98. Jaccard, S, Hayes, CT and Martínez-García, A *et al.* Two modes of change in southern ocean productivity over the past million years. *Science* 2013; **339**: 1419–23.
99. Meckler, A, Sigman, D and Gibson, K *et al.* Deglacial pulses of deep-ocean silicate into the subtropical North Atlantic Ocean. *Nature* 2013; **495**: 495–8.
100. Gingele, FX and Schmieder, F. Anomalous South Atlantic lithologies confirm global scale of unusual mid-Pleistocene climate excursion. *Earth Planet Sci Lett* 2001; **186**: 93–101.
101. Romero, O and Schmieder, F. Occurrence of thick Ethmodiscus oozes associated with a terminal mid-Pleistocene transition event in the oligotrophic subtropical South Atlantic. *Palaeogeogr Palaeocl* 2006; **235**: 321–9.
102. Thunell, RC, Poli, MS and Rio, D. Changes in deep and intermediate water properties in the western North Atlantic during marine isotope stages 11–12: evidence from ODP Leg 172. *Mar Geol* 2002; **189**: 63–77.
103. Droxler, AW and Farrell, JW. Marine Isotope Stage 11 (MIS 11): new insights for a warm future. *Global Planet Change* 2000; **24**: 1–5.
104. Tzedakis, P, Raynaud, D and McManus, J *et al.* Interglacial diversity. *Nat Geosci* 2009; **2**: 751–5.
105. Liu, C, Wang, P and Tian, J *et al.* Coccolith evidence for Quaternary nutricline variations in the southern South China Sea. *Mar Micropaleontol* 2008; **69**: 42–51.
106. Bollmann, J, Baumann, KH and Thierstein, HR. Global dominance of Gephyrocapsa coccoliths in the Late Pleistocene: selective dissolution, evolution, or global environmental change?. *Paleoceanography* 1998; **13**: 517–29.
107. Sun, H, Li, T and Sun, R. Significant changes in marine palaeoenvironments in the West Philippine Sea during the mid-Brunhes interval-evidence from coccolithophore and foraminifera assemblages, unpublished manuscript.
108. Baumann, K-H and Freitag, T. Pleistocene fluctuations in the northern Benguela Current system as revealed by coccolith assemblages. *Mar Micropaleontol* 2004; **52**: 195–215.
109. Yasuda, M, Berger, W H and Wu, G 29. Foraminifer preservation record for the last million years: Site 805, Ontong Java Plateau. In: Berger, WH, Kroenke, LW and Janecek, TR *et al.* (eds). *Proceedings of the Ocean Drilling Program, Science Results*, Vol. 130. College Station, TX: Ocean Drilling Program, 1993, 491–508.
110. Prell, WL. Oxygen and carbon isotope stratigraphy for the Quaternary of Hole 502B; evidence for two modes of isotopic variability. *Initial Rep Deep Sea* 1982; **68**: 455–64.
111. Emeis, K-C, Doose, H and Mix, AC *et al.* Alkenone sea-surface temperatures and carbon burial at Site 846 (Eastern Equatorial Pacific Ocean): the last 1.3 My. In: Pisias, NG, Mayer, LA and Janecek, TR *et al.* (eds). *Proceedings of the Ocean Drilling Program, Science Results*, Vol. 138. College Station, TX: Ocean Drilling Program, 1995, 605–13.
112. Ortiz, J, Mix, A and Harris, S *et al.* Diffuse spectral reflectance as a proxy for percent carbonate content in North Atlantic sediments. *Paleoceanography*, 1999; **14**: 171–86.
113. Harris, SE, Mix, AC and King, T. Biogenic and terrigenous sedimetations at Ceara rise, western tropical Altantic, supports Pliocene-Pleistocene deep-water linkage between hemispheres. In: Shackleton, NJ, Curry, WB and Richter, C *et al.* (eds). *Proceedings of the Ocean Drilling Program, Science Results*, Vol. 154. College Station, TX: Ocean Drilling Program, 1997, 331–45.
114. Ruddiman, WF, Raymo, M and Martinson, D *et al.* Pleistocene evolution: Northern hemisphere ice sheets and North Atlantic Ocean. *Paleoceanography* 1989; **4**: 353–412.
115. Raymo, M, Ruddiman, W and Backman, J et al. Late Pliocene variation in northern hemisphere ice sheets and North Atlantic deep water circulation. *Paleoceanography* 1989; **4**: 413–46.
116. Hall, IR, McCave, IN and Shackleton, NJ *et al.* Intensified deep Pacific inflow and ventilation in Pleistocene glacial times. *Nature* 2001; **412**: 809–12.
117. Ziegler, M, Lourens, L and Tuenter, E *et al.* High Arabian Sea productivity conditions during MIS 13—odd monsoon event or intensified overturning circulation at the end of the mid-Pleistocene transition? *Clim Past* 2010; **6**: 63–76.
118. Archer, D, Winguth, A and Lea, D *et al.* What caused the glacial/interglacial atmospheric pCO_2 cycles? *Rev Geophys* 2000; **38**: 159–89.
119. DeMaster, DJ, Leynaert, A and Queguiner, B. The silica balance in the world ocean: a reestimate. *Science* 1995; **268**: 375–79.
120. Wang, P. Global monsoon in a geological perspective. *Chinese Sci Bull* 2009; **54**: 1113–36.
121. Harrison, KG. Role of increased marine silica input on paleo-pCO_2 levels. *Paleoceanography* 2000; **15**: 292–8.
122. Berger, A. Support for the astronomical theory of climatic change. *Nature* 1977; **269**: 44–5.
123. Lourens, LJ, Sluijs, A and Kroon, D *et al.* Astronomical pacing of late Palaeocene to early Eocene global warming events. *Nature* 2005; **435**: 1083–7.
124. Katz, ME, Wright, JD and Miller, KG *et al.* Biological overprint of the geological carbon cycle. *Mar Geol* 2005; **217**: 323–38.
125. Armstrong, RA, Lee, C and Hedges, JI *et al.* A new, mechanistic model for organic carbon fluxes in the ocean based on the quantitative association of POC with ballast minerals. *Deep-Sea Res Pt II* 2001; **49**: 219–36.
126. Honjo, S, Manganini, SJ and Krishfield, RA *et al.* Particulate organic carbon fluxes to the ocean interior and factors controlling the biological pump: a synthesis of global sediment trap programs since 1983. *Prog Oceanogr* 2008; **76**: 217–85.

127. Jiao, N, Herndl, GJ and Hansell, DA *et al.* Microbial production of recalcitrant dissolved organic matter: long-term carbon storage in the global ocean. *Nat Rev Microbiol* 2010; **8**: 593–9.
128. Jiao, N and Azam, F. Microbial carbon pump and its significance for carbon sequestration in the ocean. In: Jiao, N, Azam, F and Sanders, S (eds). *Microbial Carbon Pump in the Ocean*. Washington DC: Science/AAAS, 2011, 43–5.
129. Hansell, DA. Recalcitrant dissolved organic carbon fractions. *Annu Rev Mar Sci* 2013; **5**: 421–45.
130. Edwards, KJ. Carbon cycle at depth. *Nat Geosci* 2011; **4**: 9–11.
131. Sexton, PF, Norris, RD and Wilson, PA *et al.* Eocene global warming events driven by ventilation of oceanic dissolved organic carbon. *Nature* 2011; **471**: 349–52.
132. Ridgwell, A. Evolution of the ocean's 'biological pump'. *Proc Natl Acad Sci USA* 2011; **108**: 16485–6.
133. Hansell, DA. Dissolved organic carbon reference material program. *Eos, Trans Amer Geophys Union* 2005; **86**: 318.
134. Follows, MJ, Dutkiewicz, S and Grant, S *et al.* Emergent biogeography of microbial communities in a model ocean. *Science* 2007; **315**: 1843–46.
135. Hansell, DA, Carlson, CA and Repeta, DJ *et al.* Dissolved organic matter in the ocean: a controversy stimulates new insights. *Oceanography* 2009; **22**: 202–11.
136. Karl, DM. Microbial oceanography: paradigms, processes and promise. *Nat Rev Microbiol* 2007; **5**: 759–69.
137. Karl, DM, Laws, EA and Morris, P. Global carbon cycle (communication arising): metabolic balance of the open sea. *Nature* 2003; **426**: 32.
138. Sigman, DM, Hain, MP and Haug, GH. The polar ocean and glacial cycles in atmospheric CO_2 concentration. *Nature* 2010; **466**: 47–55.
139. Anderson, R, Ali, S and Bradtmiller, L *et al.* Wind-driven upwelling in the Southern Ocean and the deglacial rise in atmospheric CO_2. *Science* 2009; **323**: 1443–8.
140. Kemp, AE and Villareal, TA. High diatom production and export in stratified waters—a potential negative feedback to global warming. *Prog Oceanogr*, doi:10.1016/j.pocean.2013.06.004.
141. Sarthou, G, Timmermans, KR and Blain, S *et al.* Growth physiology and fate of diatoms in the ocean: a review. *J Sea Res*, 2005; **53**: 25–42.
142. Matsumoto, K, Sarmiento, JL and Brzezinski, MA. Silicic acid leakage from the Southern Ocean: a possible explanation for glacial atmospheric pCO_2. *Global Biogeochem Cy* 2002; **16**: 1031.
143. Kienast, S, Kienast, M and Jaccard, S *et al.* Testing the silica leakage hypothesis with sedimentary opal records from the eastern equatorial Pacific over the last 150 kyrs. *Geophys Res Lett* 2006; **33**: L15607.
144. Bradtmiller, L, Anderson, R and Fleisher, M *et al.* Diatom productivity in the equatorial Pacific Ocean from the last glacial period to the present: a test of the silicic acid leakage hypothesis. *Paleoceanography* 2006; **21**: PA4201.
145. Yin, Q and Guo, Z. Strong summer monsoon during the cool MIS-13. *Clim Past* 2008; **4**: 29–34.
146. Yin, Q, Berger, A and Crucifix, M. Individual and combined effects of ice sheets and precession on MIS-13 climate. *Clim Past* 2009; **5**: 229–43.
147. Guo, Z, Berger, A and Yin, Q *et al.* Strong asymmetry of hemispheric climates during MIS-13 inferred from correlating China loess and Antarctica ice records. *Clim Past* 2009; **5**: 21–31.